Nonlinear Model Predictive Control of a Variable-Speed Pumped-Storage Power Plant

authored by **J.F. Mennemann, L. Marko, J. Schmidt, W. Kemmetmüller, and A. Kugi**

and published in *IEEE Transactions on Control Systems Technology*.

Nonlinear Model Predictive Control of a Variable-Speed Pumped Storage Power Plant

Jan-Frederik Mennemann, Lukas Marko, Jakob Schmidt, Wolfgang Kemmetmüller, *Member, IEEE,* and Andreas Kugi, *Senior Member, IEEE.*

***Abstract*—Optimal operation and control of (variable-speed) pumped storage power plants (PSPPs) is essential to meet the growing demands on the dynamics for the stabilization of power distribution grids with an increasing amount of renewable energy sources. Existing work on the control of PSPPs is typically based on rather simplified system models, in particular of the (long) pipeline system. In this work, a nonlinear model predictive control (MPC) strategy is proposed, which enables fast closed-loop dynamics while keeping all system constraints, including the pressure constraints along the pipeline system. The control strategy is based on a physics-based model, which enables easy parameterization and application to other plant sizes or topologies. To ensure real-time capability of the MPC strategy, a number of measures are outlined in this paper. Finally, the feasibility of the proposed control strategy is demonstrated by detailed simulation studies. An accurate tracking for fast changing desired grid powers as well as a high robustness with respect to parameter uncertainties is demonstrated.**

***Index Terms*—Variable-speed pumped storage power plant, model predictive control, physics-based model, pipeline system, pressure waves, model uncertainties, Extended Kalman Filter**

I. Introduction

CURRENT electric energy distribution systems are faced with a rapidly increasing amount of renewable energy sources, in particular wind and sun. The intermittent nature of these energy sources demands for suitable ways to store electric energy to ensure a generation-load balance. Pumped storage power plants are capable of storing large amounts of energy and thus may play an important role to balance generation and load in a grid. They are characterized by high efficiency and are able to cover fast and large changes in the energy demand. Variable-speed pumped storage power plants can bring additional flexibility with respect to these demands [1]–[4].

The optimal operation and control of variable-speed pumped storage power plants (PSPPs) is essential to meet the growing demands on the dynamics for the stabilization of power distribution grids. In the industrial state of the art, control of PSPPs is typically based on (cascaded) linear control strategies. In particular, PID control is still the prevailing method, where various extensions by fuzzy, sliding or predictive concepts have been reported in the literature, see, e.g., [1], [5], [6]. In order to systematically take into account the nonlinear system behavior, also flatness-based feedforward control was proposed in [7].

These approaches are based on rather strongly simplified system models, in particular of the long pipeline systems which connect the reservoirs with the pump-turbine. Moreover, they typically do not systematically consider the inherent nonlinearities and the (physical) constraints of the system. These effects, however, become relevant if the variable-speed pumped storage power plants are controlled at their (dynamic) limits, as this is more and more demanded by the grid and plant operator. As a first approach to take into account these effects, a generalized predictive control strategy was proposed in [8]. Therein, the dynamics of the pipeline system is taken into account by utilizing the method of characteristics (MOC) and the control strategy is based on a local linearization of the underlying nonlinear model. This control strategy does not consider the inherent constraints on the pressures in the pipeline system and only considers the speed control of the PSPP. The optimal (boundary) control of a pipeline system is, e.g., treated in [9], [10], but no coupling with a turbine and the electrical system is taken into account.

Based on this review of the literature, the following open points are addressed in this paper: (i) The control strategy has to ensure an optimal operation of the overall PSPP, in particular during quasi-stationary operation. (ii) A high-dynamic operation of the PSPP should be possible to meet short-term energy demands of the grid. In this context, the control strategy has to guarantee a safe system operation, where all relevant system constraints are systematically taken into account. In particular, the constraints on the pressure in the pipeline system are important, although they are typically neglected in the control concepts reported in the literature. (iii) The control strategy has to be robust with respect to the most important uncertain parameters of the system.

In this work, all these points are addressed by a nonlinear optimal control strategy, whose core is a nonlinear model-predictive controller for the active and reactive grid power, see, e.g., [11], [12] for the basics of NMPC. It is based on a physics-based model of the overall PSPP, where the spectral element method is applied to approximate the dynamic behavior of the long pipeline system [13]–[16].

The paper is organized as follows: The considered system and the control task are described in detail in Section II.

J.-F. Mennemann and J. Schmidt were with the Automation & Control Institute, TU Wien, Austria, e-mail: jfmennemann@gmx.de, jakob.schmidt1@protonmail.com.

L. Marko is with the Christian Doppler Laboratory for Model-Based Process Control in the Steel Industry, Automation & Control Institute, TU Wien, Austria, e-mail: marko@acin.tuwien.ac.at.

W. Kemmetmüller is with the Automation & Control Institute, TU Wien, Austria, e-mail: kemmetmueller@acin.tuwien.ac.at.

A. Kugi is with the Automation & Control Institute, TU Wien, Austria, and the Center for Vision, Automation & Control, Austrian Institute of Technology, Austria, e-mail: kugi@acin.tuwien.ac.at.

Post-print version of the article: J. Mennemann, L. Marko, J. Schmidt, W. Kemmetmüller, and A. Kugi, “Nonlinear model predictive control of a variable-speed pumped-storage power plant,” *IEEE Transactions on Control Systems Technology*, vol. 29, no. 2, pp. 645–660, 2021. DOI: 10.1109/TCST.2019.2956910

Section III summarizes the mathematical model of the system. The overall control strategy, consisting of a static optimizer, a model predictive control (MPC) concept and an Extended Kalman Filter (EKF), is developed in Section IV. In Section V, essential details for the efficient real-time implementation of the proposed control strategy are discussed. The accuracy, feasibility and effectiveness of the proposed control approach is demonstrated by extensive simulation studies in Section VI.

II. System Description and Control Task

Fig. 1 depicts a sketch of the variable-speed pumped storage power plant (PSPP). In the studied turbine mode[1], water flows from the upper reservoir via a pipeline system and two Francis type turbines to the lower reservoir. The turbines of the identical plant units I and II drive doubly-fed induction machines (DFIM), which are controlled by voltage source converters (VSC) comprising a grid side inverter (GSI) and rotor side inverter (RSI). This setup allows for a variable-speed operation of the turbines, which is meaningful to improve the overall efficiency of the plant, in particular for part load operation [4].

The main control task for this system is to provide active and reactive power (P_{g}, Q_{g}) according to the grid operators demand, while minimizing the overall losses of the system. To do so, the voltages of the VSC (rotor voltages $U_{\mathrm{d,r}}$, $U_{\mathrm{q,r}}$, transformer voltages $U_{\mathrm{d,t}}$, $U_{\mathrm{q,t}}$) and the guide vane position χ of the turbines are utilized as control inputs. This control task is particularly challenging due to the following reasons: (i) The pipeline system covers a length of more than $2000\,\mathrm{m}$. Thus, in dynamic operation of the plant, the distributed-parameter character of the pipeline system has to be taken into account. (ii) The system, in particular the turbine, exhibits a pronounced nonlinear behavior. (iii) The operation of the system is restricted by several limitations, e.g., with respect to maximum currents, voltages, speed, power and the pressures in the pipelines.

To solve this control task, a model predictive control (MPC) strategy is proposed in this paper. For the derivation of this MPC strategy, a number of (simplifying) assumptions are made: (i) The overall PSPP consists of two identical plant units, which are connected to the same upper and lower reservoir. An earlier study on the optimal stationary operation of this plant showed that in turbine mode, optimal operation is typically characterized by identical operation of both plant units [4]. Thus, it is reasonable to assume identical operation of both plant units for the dynamic operation as well. (ii) Typically, a fast local controller is utilized to control the direct current link voltage U_{dc} of the VSC to a constant value. Thus, the control of the VSC by $U_{\mathrm{d,t}}$ and $U_{\mathrm{q,t}}$ is not considered in the control strategy and only the rotor voltages $U_{\mathrm{d,r}}$ and $U_{\mathrm{q,r}}$ serve as control inputs. (iii) The losses and the influence on the overall dynamic behavior of the converter transformer (CT) and the step-up transformer (ST) are small in normal operation. Thus, an idealized model for the converter transformer is used and the step-up transformer is neglected.

[1] Although the paper concentrates on the turbine mode, the mathematical model and the proposed control strategy are directly applicable to the pumping mode with only minor changes.

III. Mathematical Model

In order to efficiently apply model predictive control techniques, a mathematical model tailored to the specific control task is required. In particular, a good compromise between model accuracy and complexity has to be found. The authors studied the control oriented mathematical modeling of the considered plant in the previous publications [4], [15], [16]. The model equations given in this section are a short summary of this model and are given for the sake of completeness. The detailed derivation and discussion of the model equations can be found in [4], [15], [16].

A. Hydraulic Part

An illustration of the spatial positions and the interconnection of the pipelines is given in Fig. 2. In this figure, the spatial positions are represented using an (x, y, z)-coordinate frame, with y being oriented in the opposite direction of gravitational acceleration. According to Fig. 1, the first pipeline is connected to the upper reservoir (pressure $p_{\mathrm{res,t}}$) and the sixth pipeline is connected to the lower reservoir (pressure $p_{\mathrm{res,b}}$).

For the mathematical modeling, the pipelines are parameterized as a function of their arc length $s_i \in [0, L_i]$, where L_i denotes the length of the ith pipeline, $i = 1, \ldots, 6$. Each pipeline is further characterized by its inclination $\alpha_i(s_i)$, diameter $D_i(s_i)$ and its wave propagation speed $c_i(s_i)$, see Fig. 3. As stated before it is assumed that the two plant units are identical and thus the coefficient functions of the third and fifth pipeline coincide with those of the second and fourth one, respectively.

Wave propagation effects in pipelines are a well known phenomenon which are extensively studied in the literature, see, e.g., [17]–[21]. The dynamic behavior of a pipeline i, $i = 1, \ldots, 6$, is typically described by the volumetric flow q_i and the piezometric height h_i

$$h_i = \frac{p_i}{\rho g} + y_i, \tag{1}$$

with the pressure p_i, the mass density ρ of water, the gravitional acceleration g and the height profile y_i. The height profile is determined from the inclination α_i by

$$y_i(s_i) = y_i^0 + \int_0^{s_i} \sin(\alpha_i(s))\,\mathrm{d}s. \tag{2}$$

The time evolution of the piezometric head h_i and the volume flow q_i of the ith pipeline is governed by a system of hyperbolic partial differential equations (PDE) [17], [20], [22]

$$\frac{\partial}{\partial t}\begin{bmatrix} h_i \\ q_i \end{bmatrix} + \begin{bmatrix} 0 & c_i^2/(gA_i) \\ gA_i & 0 \end{bmatrix} \frac{\partial}{\partial s}\begin{bmatrix} h_i \\ q_i \end{bmatrix} = -\begin{bmatrix} 0 \\ r_i q_i |q_i| \end{bmatrix}, \tag{3}$$

where $A_i = \pi(D_i/2)^2$ denotes the cross-sectional area and $r_i = f_\lambda/(2D_iA_i)$ describes the pipe friction, with the Darcy-Weisbach friction factor f_λ. In general, this simple static friction model tends to underestimate pipe friction in case of very fast dynamic changes, see, e.g. [21], [23]. The influence of pipe friction is, however, small compared to the large variations of the pressure and volume flow in dynamic operation. The main requirement is to accurately cover the small pipe losses in stationary operation to ensure correct

Post-print version of the article: J. Mennemann, L. Marko, J. Schmidt, W. Kemmetmüller, and A. Kugi, "Nonlinear model predictive control of a variable-speed pumped-storage power plant," *IEEE Transactions on Control Systems Technology*, vol. 29, no. 2, pp. 645–660, 2021. DOI: 10.1109/TCST.2019.2956910
The content of this post-print version is identical to the published paper but without the publisher's final layout or copy editing.

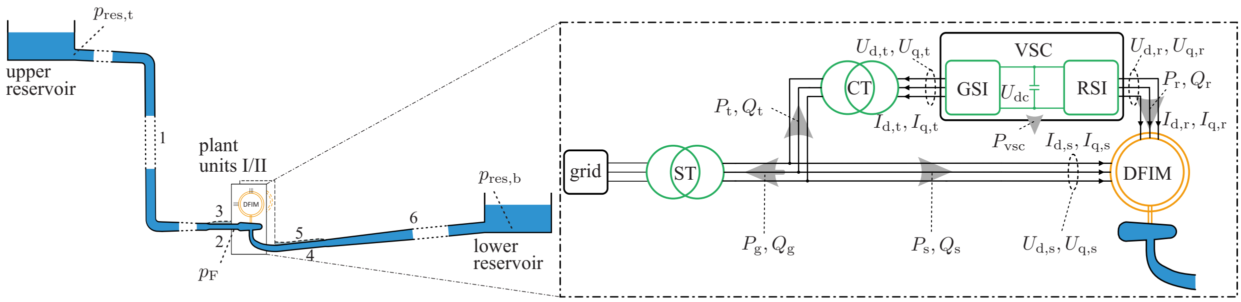

Fig. 1. Sketch of the overall pumped storage power plant under consideration [4].

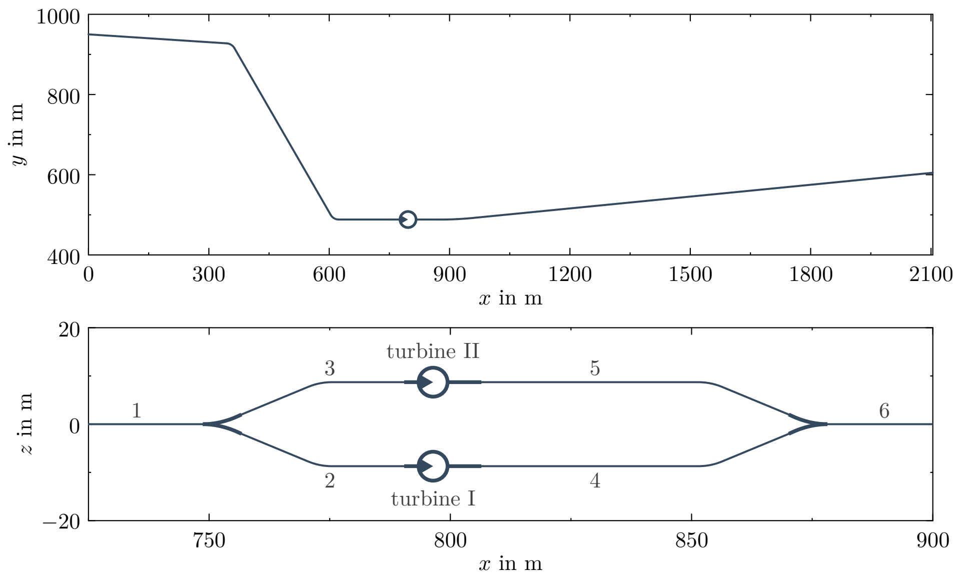

Fig. 2. Spatial positions of the pipelines and turbines corresponding to the pumped storage power plant considered in this article [16].

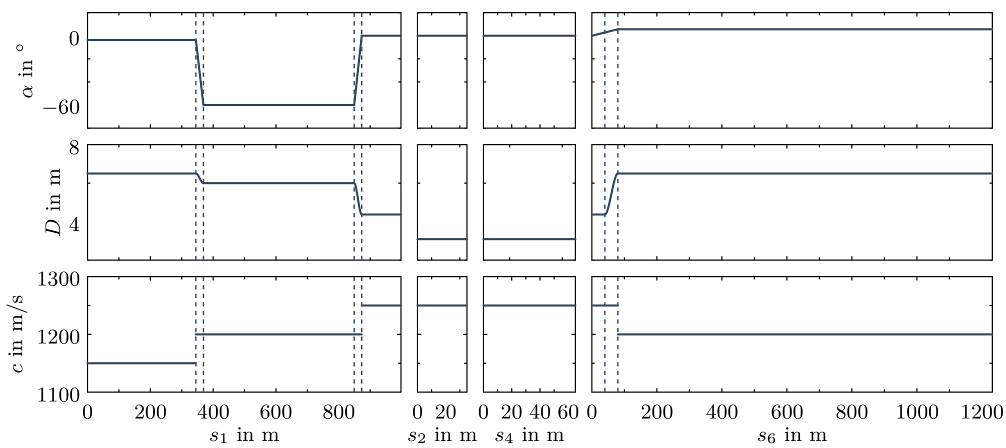

Fig. 3. Inclination α_i, diameter D_i and wave propagation speed c_i of the pipeline system given in Fig. 2. In the semi-discretization by means of the spectral element method (SEM), each pipeline is subdivided into one or more elements, which are indicated by dashed vertical lines [16].

Post-print version of the article: J. Mennemann, L. Marko, J. Schmidt, W. Kemmetmüller, and A. Kugi, "Nonlinear model predictive control of a variable-speed pumped-storage power plant," *IEEE Transactions on Control Systems Technology*, vol. 29, no. 2, pp. 645–660, 2021. DOI: 10.1109/TCST.2019.2956910
The content of this post-print version is identical to the published paper but without the publisher's final layout or copy editing.

stationary operating points [4]. This is possible by the utilized simple static friction model.

The MPC relies on a low-dimensional but accurate approximation of the PDE system (3). To this end, (3) is discretized by means of the spectral element method (SEM), see, e.g., [16] for details on the application of this method to hydraulic pipelines. The piezometric height h_i and the volume flow q_i are replaced by the approximations

$$h_i(s_i,t) = \sum_{j=1}^{J_i} h_{i,j}(t)\phi_{i,j}(s_i), \tag{4a}$$

$$q_i(s_i,t) = \sum_{j=1}^{J_i} q_{i,j}(t)\phi_{i,j}(s_i), \tag{4b}$$

where $\phi_{i,1},\dots,\phi_{i,J_i}$ denotes a set of basis functions corresponding to a subdivision of the ith pipeline in J_i elements. Collecting all coefficient functions in

$$\boldsymbol{h}_i = \left[h_{i,1},\dots,h_{i,J_i}\right]^T, \quad \boldsymbol{q}_i = \left[q_{i,1},\dots,q_{i,J_i}\right]^T, \tag{5}$$

the semi-discretization of (3) by means of the SEM can be written as [16]

$$\boldsymbol{M}_{\epsilon,i}\frac{\mathrm{d}\boldsymbol{h}_i}{\mathrm{d}t} = \boldsymbol{S}_i\boldsymbol{q}_i + q_{i,1}^*\boldsymbol{e}_{i,1} - q_{i,J_i}^*\boldsymbol{e}_{i,J_i}, \tag{6a}$$

$$\boldsymbol{M}_{\mu,i}\frac{\mathrm{d}\boldsymbol{q}_i}{\mathrm{d}t} = \boldsymbol{S}_i\boldsymbol{h}_i + h_{i,1}^*\boldsymbol{e}_{i,1} - h_{i,J_i}^*\boldsymbol{e}_{i,J_i} - \boldsymbol{M}_{r,i}\boldsymbol{q}_i|\boldsymbol{q}_i|. \tag{6b}$$

Here, $\boldsymbol{e}_{i,1}$ and $\boldsymbol{e}_{i,J_i}$ represent J_i-dimensional vectors

$$\boldsymbol{e}_{i,1} = \left[1,0,\dots,0\right]^T, \quad \boldsymbol{e}_{i,J_i} = \left[0,\dots,0,1\right]^T \tag{7}$$

and $\boldsymbol{q}_i|\boldsymbol{q}_i|$ denotes the element-wise multiplication of the two vectors $\boldsymbol{q}_i$ and $|\boldsymbol{q}_i|$. The variables $q_{i,1}^*$, q_{i,J_i}^*, $h_{i,1}^*$, and h_{i,J_i}^* are subsequently used to implement the boundary conditions of the individual pipelines. For a comprehensive discussion of the basis functions, the mass matrices $\boldsymbol{M}_{\epsilon,i}$ and $\boldsymbol{M}_{\mu,i}$, the matrix $\boldsymbol{M}_{r,i}$, and the stiffness matrix $\boldsymbol{S}_i$ the reader is referred to [16], where also an in-depth numerical convergence analysis is presented.

Similar to the results in [16], the second and fourth pipeline are discretized by means of a single element, whereas the first and sixth pipeline are discretized using five and three elements, respectively, see Fig. 3. The corresponding polynomial degrees of the shape functions on these elements are chosen as

$$(N_{1,1},N_{1,2},N_{1,3},N_{1,4},N_{1,5}) = (3,1,3,1,2), \tag{8a}$$

$$N_{2,1} = N_{4,1} = 1, \tag{8b}$$

$$(N_{6,1},N_{6,2},N_{6,3}) = (1,1,8). \tag{8c}$$

This choice of the elements and the shape functions is based on the observation that, even for fast transients, the spatial distribution of the pressure and the volume flow along the pipeline system remains sufficiently smooth, see [16] for a detailed discussion. The chosen discretization gives $2\times(11+2+2+11) = 52$ dynamical variables to approximate the piezometric heights h_i and the volume flows q_i, $i\in\{1,2,4,6\}$.

The boundary conditions of the system are implemented in a weak sense using a numerically stable upwind discretization [16]. To this end, the variables $q_{i,1}^*$, q_{i,J_i}^*, $h_{i,1}^*$ and h_{i,J_i}^* in (6) have to be adequately defined. The first set of boundary conditions results from the coupling of the pipelines to the reservoirs. It is assumed that within the time-scale of the dynamic operation of the plant, the corresponding piezometric heights $h_{\mathrm{res,t}} = p_{\mathrm{res,t}}/(\rho g) + y_1(0)$ and $h_{\mathrm{res,b}} = p_{\mathrm{res,b}}/(\rho g) + y_6(L_6)$ are constant. Then, these boundary conditions can be written in the form [16]

$$q_{1,1}^* = q_{1,1} - gA_1(0)(h_{1,1} - h_{\mathrm{res,t}})/c_1(0), \tag{9a}$$

$$h_{1,1}^* = h_{\mathrm{res,t}}, \tag{9b}$$

$$q_{6,J_6}^* = q_{6,J_6} - gA_6(L_6)(h_{\mathrm{res,b}} - h_{6,J_6})/c_6(L_6), \tag{9c}$$

$$h_{6,J_6}^* = h_{\mathrm{res,b}}, \tag{9d}$$

with $J_6 = 11$ for the considered system. For the description of the branching of pipeline 1 into pipelines 2 and 3, identical operation of the two plant units is considered. This means that the volume flows and piezometric heights of pipeline 3 are identical to those of pipeline 2. Thus, it is sufficient to consider pipeline 2 in the model and utilize the following formulation of the boundary conditions

$$q_{1,J_1}^* = 2q_{2,1}, \tag{10a}$$

$$h_{1,J_1}^* = h_{1,J_1} - c_1(L_1)(2q_{2,1} - q_{1,J_1})/(gA_1(L_1)), \tag{10b}$$

$$q_{2,1}^* = q_{2,1} + gA_2(0)(h_{1,J_1} - h_{2,1})/c_2(0), \tag{10c}$$

$$h_{2,1}^* = h_{1,J_1}, \tag{10d}$$

$J_1 = 11$. Equivalently, the branching of pipeline 6 into pipelines 4 and 5 is described by the boundary conditions

$$q_{4,J_4}^* = q_{4,J_4} - gA_4(L_4)(h_{6,1} - h_{4,J_4})/c_4(L_4), \tag{11a}$$

$$h_{4,J_4}^* = h_{6,1}, \tag{11b}$$

$$q_{6,1}^* = 2q_{4,J_4}, \tag{11c}$$

$$h_{6,1}^* = h_{6,1} + c_6(0)(2q_{4,J_4} - q_{6,1})/(gA_6(0)), \tag{11d}$$

$J_4 = 2$. Finally, the coupling of pipeline 2 and 4 to the Francis turbines reads as

$$q_{2,J_2}^* = q_{\mathrm{F}}, \tag{12a}$$

$$h_{2,J_2}^* = h_{2,J_2} - c_2(L_2)(q_{\mathrm{F}} - q_{2,J_2})/(gA_2(L_2)), \tag{12b}$$

$$q_{4,1}^* = q_{\mathrm{F}}, \tag{12c}$$

$$h_{4,1}^* = h_{4,1} + c_4(0)(q_{\mathrm{F}} - q_{1,4})/(gA_4(0)), \tag{12d}$$

where q_{F} denotes the volume flow through the Francis turbine and $J_2 = 2$. The volume flow q_{F} is modeled by means of the nonlinear algebraic equation [4], [16]

$$\begin{aligned} 0 = W_{\mathrm{h}}(\chi,\vartheta)\left[(q_{\mathrm{F}}/q_{\mathrm{ref}})^2 + (\omega/\omega_{\mathrm{ref}})^2\right]h_{\mathrm{ref}} - (h_{2,J_2}^* - h_{4,1}^*) \\ - q_{\mathrm{F}}^2\left[(1/A_2(L_2))^2 - (1/A_4(0))^2\right]/(2g), \end{aligned} \tag{13}$$

where ω and χ denote the angular velocity and the guide vane position, respectively, of the (synchronously operated) turbines, and

$$\vartheta = \arctan\left(\frac{q_{\mathrm{F}}/q_{\mathrm{ref}}}{\omega/\omega_{\mathrm{ref}}}\right), \tag{14}$$

denotes a dimensionless variable which is needed to evaluate the characteristic map $W_{\mathrm{h}}(\chi,\vartheta)$ of the turbine, see, e.g., [4], [24]. The characteristic parameters of the turbine h_{ref}, q_{ref} and ω_{ref} are listed in Table I. It has to be noted that due

Post-print version of the article: J. Mennemann, L. Marko, J. Schmidt, W. Kemmetmüller, and A. Kugi, "Nonlinear model predictive control of a variable-speed pumped-storage power plant," *IEEE Transactions on Control Systems Technology*, vol. 29, no. 2, pp. 645–660, 2021. DOI: 10.1109/TCST.2019.2956910

to the assumed identical operation of both turbines, (9)-(13) constitute a simplification of the model given in [16].

The guide vane position χ and its adjustment speed $v_\chi = \dot{\chi}$ are subject to the constraints

$$\chi^{\mathrm{lb}} \leqslant \chi \leqslant \chi^{\mathrm{ub}}, \tag{15a}$$
$$v_\chi^{\mathrm{lb}} \leqslant v_\chi \leqslant v_\chi^{\mathrm{ub}}. \tag{15b}$$

As discussed before, one major limitation of the system operation is given by the constraints on the pressure along the pipeline system. These bounds can be equivalently formulated in the piezometric heights as

$$h_i^{\mathrm{lb}} \leqslant h_i \leqslant h_i^{\mathrm{ub}}, \tag{16}$$

with

$$h_i^{\mathrm{lb}} = \frac{p_i^{\mathrm{lb}}}{\rho g} + y_i, \qquad h_i^{\mathrm{ub}} = \frac{p_i^{\mathrm{ub}}}{\rho g} + y_i. \tag{17}$$

To avoid cavitation of the water in the pipelines, the lower pressure bound is set to $p_i^{\mathrm{lb}} = 1\,\mathrm{bar}$, $i = 1, 2, 4, 6$. The upper bound is basically defined by the construction (i.e. by the material and thickness) of the pipe walls. Typically, they are designed to withstand pressures which are a certain factor σ above the stationary pressure distribution p_i^0 in the pipeline i. Thus, the upper bound is defined as $p_i^{\mathrm{ub}} = \sigma p_i^0 + \Delta p^b$, $i = 1, 2, 4, 6$, where realistic values of the parameters σ and Δp^b are summarized in Table I.

B. Mechanical and Electrical Part

The turbine is rigidly coupled to the rotor of the doubly-fed induction machine (DFIM). Applying the conservation of angular momentum results in

$$\frac{\mathrm{d}\omega}{\mathrm{d}t} = \frac{1}{J}(M_{\mathrm{h}} - M_{\mathrm{e}} - M_{\mathrm{f}}). \tag{18}$$

Here, J is the overall moment of inertia of the turbine and the rotor, M_{h} is the turbine torque, M_{e} the torque of the DFIM and M_{f} denotes the friction torque. The turbine torque can be described by [4], [25]

$$M_{\mathrm{h}} = W_{\mathrm{b}}(\chi, \vartheta)\big[(q_{\mathrm{F}}/q_{\mathrm{ref}})^2 + (\omega/\omega_{\mathrm{ref}})^2\big]M_{\mathrm{ref}}, \tag{19}$$

where $W_{\mathrm{b}}(\chi, \vartheta)$ is a characteristic map which describes the turbine. The friction torque is composed of Coulomb friction M_{c} and ventilation losses $d_{\mathrm{v}}\omega^2$, i.e. $M_{\mathrm{f}} = M_{\mathrm{c}} + d_{\mathrm{v}}\omega^2$. Finally, the torque of the DFIM reads as

$$M_{\mathrm{e}} = -\frac{3}{2} p L_{\mathrm{m}}(I_{\mathrm{q,s}} I_{\mathrm{d,r}} - I_{\mathrm{q,r}} I_{\mathrm{d,s}}), \tag{20}$$

with the stator and rotor currents $I_{\mathrm{q,s}}$, $I_{\mathrm{d,s}}$ and $I_{\mathrm{q,r}}$, $I_{\mathrm{d,r}}$, respectively, the number of pole pairs p and the main inductance L_{m}. Here and henceforth all electric quantities are described using a dq-coordinate system.

Remark 1: The characteristic maps $W_{\mathrm{b}}(\chi, \vartheta)$ and $W_{\mathrm{h}}(\chi, \vartheta)$ of the turbine are approximated by sums of Gaussians [26]

$$W(\chi, \vartheta) = \sum_{m=1}^{M} A_m \exp\left(-\frac{(\chi - \chi_m)^2}{2\sigma_{\chi,m}^2} - \frac{(\vartheta - \vartheta_m)^2}{2\sigma_{\vartheta,m}^2}\right),$$

where W represents one of the characteristic maps W_{b} or W_{h}. Both, W_{b} and W_{h} are approximated using $M = 40$ Gaussians with individual parameters A_m, χ_m, $\sigma_{\chi,m}$, ϑ_m, and $\sigma_{\vartheta,m}$, which are found by minimizing the squared approximation error. This smooth approximation allows to easily obtain the gradients of W_{b} and W_{h} with respect to their arguments, which is beneficial for the solution of optimization problems. Furthermore, it features reduced computation times in comparison to typical two dimensional spline interpolation.

A detailed description of the mathematical model of the considered electrical system depicted in Fig. 1 is presented in [4]. Compared to this model, a number of additional (simplifying) assumptions are made for the derivation of a mathematical model tailored to the needs of a controller design utilizing MPC: (i) Iron losses of the DFIM are neglected. (ii) It is assumed that the voltage source converter (VSC) is controlled by a subordinate control strategy such that the dc-link voltage U_{dc} can be assumed constant and that the reactive power Q_{t} at the grid side inverter (GSI) is zero. (iii) An idealized behavior of the step-up transformer (ST) and the converter transformer (CT) is assumed, neglecting any losses. This implies that the stator voltages $U_{\mathrm{d,s}}$, $U_{\mathrm{q,s}}$ are directly linked to the grid voltages, and the voltages $U_{\mathrm{d,t}}$, $U_{\mathrm{q,t}}$ are directly linked to the stator voltages by fixed coupling factors. (iv) It is assumed that the grid voltage and frequency are constant within the considered prediction horizon of the MPC. The influence of these simplifications was proven to be small for the considered plant by simulations on a detailed model in [4].

Given these assumptions, the DFIM is described by

$$\frac{\mathrm{d}}{\mathrm{d}t}\begin{bmatrix} I_{\mathrm{d,s}} \\ I_{\mathrm{q,s}} \\ I_{\mathrm{d,r}} \\ I_{\mathrm{q,r}} \end{bmatrix} = \boldsymbol{A}_{\mathrm{D1}}\begin{bmatrix} I_{\mathrm{d,s}} \\ I_{\mathrm{q,s}} \\ I_{\mathrm{d,r}} \\ I_{\mathrm{q,r}} \end{bmatrix} + \omega \boldsymbol{A}_{\mathrm{D2}}\begin{bmatrix} I_{\mathrm{d,s}} \\ I_{\mathrm{q,s}} \\ I_{\mathrm{d,r}} \\ I_{\mathrm{q,r}} \end{bmatrix} + \boldsymbol{G}_{\mathrm{D}}\begin{bmatrix} U_{\mathrm{d,s}} \\ U_{\mathrm{q,s}} \\ U_{\mathrm{d,r}} \\ U_{\mathrm{q,r}} \end{bmatrix}, \tag{21}$$

where the rotor voltages $U_{\mathrm{d,r}}$, $U_{\mathrm{q,r}}$ are the control inputs of the MPC and a suitable choice of the dq-system results in $U_{\mathrm{d,s}} = 12.25\,\mathrm{kV}$ and $U_{\mathrm{q,s}} = 0\,\mathrm{V}$. The matrices $\boldsymbol{A}_{\mathrm{D1}}$, $\boldsymbol{A}_{\mathrm{D2}}$, and $\boldsymbol{G}_{\mathrm{D}}$ are given in Appendix A, see, e.g., [27].

The active and reactive grid output power, whose control is the main objective of the MPC, are given by

$$P_{\mathrm{g}} = -2\,(P_{\mathrm{s}} + P_{\mathrm{t}}), \tag{22a}$$
$$Q_{\mathrm{g}} = -2\,(Q_{\mathrm{s}} + Q_{\mathrm{t}}) = -2Q_{\mathrm{s}}, \tag{22b}$$

where, according to the previous assumptions, $Q_{\mathrm{t}} = 0$ is utilized. Using $U_{\mathrm{q,s}} = 0$, the stator powers read as

$$P_{\mathrm{s}} = \frac{3}{2} U_{\mathrm{d,s}} I_{\mathrm{d,s}}, \qquad Q_{\mathrm{s}} = -\frac{3}{2} U_{\mathrm{d,s}} I_{\mathrm{q,s}}, \tag{23}$$

Similarly, utilizing $U_{\mathrm{d,s}} = k_{\mathrm{ts}} U_{\mathrm{d,t}}$, $U_{\mathrm{q,s}} = k_{\mathrm{ts}} U_{\mathrm{q,t}} = 0$, the powers at the converter transformer are given by

$$P_{\mathrm{t}} = \frac{3}{2}\frac{U_{\mathrm{d,s}}}{k_{\mathrm{ts}}} I_{\mathrm{d,t}}, \qquad Q_{\mathrm{t}} = -\frac{3}{2}\frac{U_{\mathrm{d,s}}}{k_{\mathrm{ts}}} I_{\mathrm{q,t}}, \tag{24}$$

where k_{ts} is the coupling factor of the converter transformer. Note that the assumption $Q_{\mathrm{t}} = 0$ immediately yields $I_{\mathrm{q,t}} = 0$.

The voltage source converter is described by applying the balance of (active) power in the form

$$0 = P_{\mathrm{t}} - P_{\mathrm{r}} - P_{\mathrm{cl}}, \tag{25}$$

Post-print version of the article: J. Mennemann, L. Marko, J. Schmidt, W. Kemmetmüller, and A. Kugi, "Nonlinear model predictive control of a variable-speed pumped-storage power plant," *IEEE Transactions on Control Systems Technology*, vol. 29, no. 2, pp. 645–660, 2021. DOI: 10.1109/TCST.2019.2956910
The content of this post-print version is identical to the published paper but without the publisher's final layout or copy editing.

with the rotor power

$$P_{\mathrm{r}} = \frac{3}{2}(U_{\mathrm{d,r}}I_{\mathrm{d,r}} + U_{\mathrm{q,r}}I_{\mathrm{q,r}}) \tag{26}$$

and the stationary losses of the VSC [4]

$$P_{\mathrm{cl}} = k_{\mathrm{t},1}I_{\mathrm{t}} + k_{\mathrm{t},2}I_{\mathrm{t}}^2 + k_{\mathrm{r},1}I_{\mathrm{r}} + k_{\mathrm{r},2}I_{\mathrm{r}}^2 + P_{\mathrm{cl0}}. \tag{27}$$

Therein, the amplitudes of the rotor and grid side converter currents are utilized, which are defined as

$$I_{\mathrm{t}} = \sqrt{I_{\mathrm{d,t}}^2 + I_{\mathrm{q,t}}^2} = |I_{\mathrm{d,t}}|, \tag{28a}$$

$$I_{\mathrm{r}} = \sqrt{I_{\mathrm{d,r}}^2 + I_{\mathrm{q,r}}^2}. \tag{28b}$$

The operation of the electric system is restricted to the constraints of the rotor voltage and rotor current amplitudes $U_{\mathrm{r}} = \sqrt{U_{\mathrm{d,r}}^2 + U_{\mathrm{q,r}}^2}$ and I_{r}, respectively, and the rotor power P_{r}

$$U_{\mathrm{r}} \leqslant U_{\mathrm{r}}^{\mathrm{ub}}, \qquad I_{\mathrm{r}} \leqslant I_{\mathrm{r}}^{\mathrm{ub}}, \qquad P_{\mathrm{r}}^{\mathrm{lb}} \leqslant P_{\mathrm{r}} \leqslant P_{\mathrm{r}}^{\mathrm{ub}}, \tag{29}$$

with the bounds $U_{\mathrm{r}}^{\mathrm{ub}}$, $I_{\mathrm{r}}^{\mathrm{ub}}$, $P_{\mathrm{r}}^{\mathrm{lb}}$, and $P_{\mathrm{r}}^{\mathrm{ub}}$ given in Table I.

TABLE I
MODEL PARAMETERS OF THE SYSTEM.

Symbol	Value	Unit	Symbol	Value	Unit
g	9.81	m/s^2	d_{v}	12.38	s^2 N m
ρ	1000	kg/m^3	$U_{\mathrm{d,s}}$	12.25	kV
f_λ	6.5×10^{-3}	1	$U_{\mathrm{q,s}}$	0	V
$p_{\mathrm{res,t}}$	6.5	bar	p	7	1
$p_{\mathrm{res,b}}$	1.5	bar	L_{m}	13.99	mH
h_{ref}	313.4	m	P_{cl0}	72	kW
q_{ref}	44.68	m^3/s	$k_{\mathrm{t},1}$	19.17	W/A
ω_{ref}	42.14	rad/s	$k_{\mathrm{t},2}$	3.08	mW/A^2
M_{ref}	3.03×10^6	N m	$k_{\mathrm{r},1}$	35.94	W/A
J	700×10^3	kg/m^2	$k_{\mathrm{r},2}$	5.78	mW/A^2
M_{c}	1.68×10^4	N m	k_{ts}	5	1
σ	1.3	1	Δp^b	0.5	bar
R_{s}	2.26	mΩ	R_{r}	6.82	mΩ
L_{s}	8.03	mH	L_{r}	27.17	mH
ω_{s}	$2\pi 50$	rad/s			
$U_{\mathrm{r}}^{\mathrm{ub}}$	$\sqrt{2/3}\ 3.3$	kV	$I_{\mathrm{r}}^{\mathrm{ub}}$	$\sqrt{2}\ 6.3$	kA
$P_{\mathrm{r}}^{\mathrm{lb}}$	-14	MW	$P_{\mathrm{r}}^{\mathrm{ub}}$	14	MW

C. Overall System Model

The combination of the sub-models of the hydraulic, mechanical and electrical parts yields a system of differential-algebraic equations (DAEs) of the form

$$\dot{\boldsymbol{x}} = \boldsymbol{f}(\boldsymbol{x}, \boldsymbol{z}, \boldsymbol{u}), \tag{30a}$$

$$\boldsymbol{0} = \boldsymbol{g}(\boldsymbol{x}, \boldsymbol{z}, \boldsymbol{u}), \tag{30b}$$

where

$$\boldsymbol{x} = \left[\boldsymbol{h}_1^T, \boldsymbol{q}_1^T, \boldsymbol{h}_2^T, \boldsymbol{q}_2^T, \boldsymbol{h}_4^T, \boldsymbol{q}_4^T, \boldsymbol{h}_6^T, \boldsymbol{q}_6^T, \omega, I_{\mathrm{d,s}}, I_{\mathrm{q,s}}, I_{\mathrm{d,r}}, I_{\mathrm{q,r}}\right]^T \tag{30c}$$

$$\boldsymbol{z} = \left[q_{\mathrm{F}}, I_{\mathrm{d,t}}\right]^T \tag{30d}$$

denote the state variables and the algebraic variables, respectively. The control inputs $\boldsymbol{u}$ read as

$$\boldsymbol{u} = \left[U_{\mathrm{d,r}}, U_{\mathrm{q,r}}, \chi\right]^T. \tag{30e}$$

IV. Control Strategy

The main control objective is the optimal and safe dynamical operation of the PSPP. Optimal operation is characterized by minimizing the system losses and tracking the desired active and reactive grid power $P_{\mathrm{g}}^{\mathrm{d}}$ and $Q_{\mathrm{g}}^{\mathrm{d}}$, respectively, as good as possible. These two demands are, to a certain extent, contradictory, since exact tracking of fast changing grid power references will increase the system losses. This makes it difficult to directly tackle this control problem with a model predictive control strategy (MPC) only. The main focus of this paper is the accurate tracking of fast changing desired reference values of the grid power. In these situations, the losses of the system are only of secondary importance. Thus, the MPC part of the overall control strategy depicted in Fig. 4 will focus on the tracking task, where a safe operation of the system is ensured by systematically taking into account all system constraints (15), (16), and (29). To allow for an energy optimal operation of the PSPP in times with slow or no changes in the desired grid power, the MPC concept is combined with a static optimizer to calculate stationary operating points $\boldsymbol{x}^*, \boldsymbol{z}^*, \boldsymbol{u}^*$, which minimizes the system losses. It will be shown later that this combination allows to accurately track fast changing desired grid powers while maintaining energy optimal operation of the PSPP in the quasi-stationary case. The overall control strategy is completed by an Extended Kalman Filter (EKF), which estimates non-measurable states and uncertain parameters, cf. Fig. 4.

A. Optimal Stationary Operating Points

The task of the static optimizer is to calculate optimal stationary operating points which minimize the system losses. The desired values of the active and reactive grid power $P_{\mathrm{g}}^{\mathrm{d}}$ and $Q_{\mathrm{g}}^{\mathrm{d}}$, respectively, are defined by the operator of the PSPP. To avoid meaningless fast changes, rate limited values P_{g}^* and Q_{g}^* are utilized in the optimization.

A stationary operating point is defined by the corresponding values of the state variables $\boldsymbol{x}$, the algebraic variables $\boldsymbol{z}$ and the control input $\boldsymbol{u}$. The optimal values $\boldsymbol{x}^*$, $\boldsymbol{z}^*$, $\boldsymbol{u}^*$ follow from the solution of the optimization problem

$$\min_{\boldsymbol{x},\boldsymbol{z},\boldsymbol{u}} \quad P_{\mathrm{in}}(\boldsymbol{x}, \boldsymbol{z}, \boldsymbol{u}) - P_{\mathrm{out}}(\boldsymbol{x}, \boldsymbol{z}, \boldsymbol{u}) \tag{31a}$$

subject to

$$P_{\mathrm{g}}(\boldsymbol{x}, \boldsymbol{z}, \boldsymbol{u}) = P_{\mathrm{g}}^*, \tag{31b}$$

$$Q_{\mathrm{g}}(\boldsymbol{x}, \boldsymbol{z}, \boldsymbol{u}) = Q_{\mathrm{g}}^*, \tag{31c}$$

$$\boldsymbol{f}(\boldsymbol{x}, \boldsymbol{z}, \boldsymbol{u}) = \boldsymbol{0}, \tag{31d}$$

$$\boldsymbol{g}(\boldsymbol{x}, \boldsymbol{z}, \boldsymbol{u}) = \boldsymbol{0} \tag{31e}$$

and the inequality constraints in (15a) and (29)[2]. Here, the input power P_{in} is given by the difference of the power of the

[2] Note that the remaining inequality constraints (15b) and (16) are not relevant here since they cannot be violated in stationary operation of the plant.

Post-print version of the article: J. Mennemann, L. Marko, J. Schmidt, W. Kemmetmüller, and A. Kugi, "Nonlinear model predictive control of a variable-speed pumped-storage power plant," *IEEE Transactions on Control Systems Technology*, vol. 29, no. 2, pp. 645–660, 2021. DOI: 10.1109/TCST.2019.2956910
The content of this post-print version is identical to the published paper but without the publisher's final layout or copy editing.

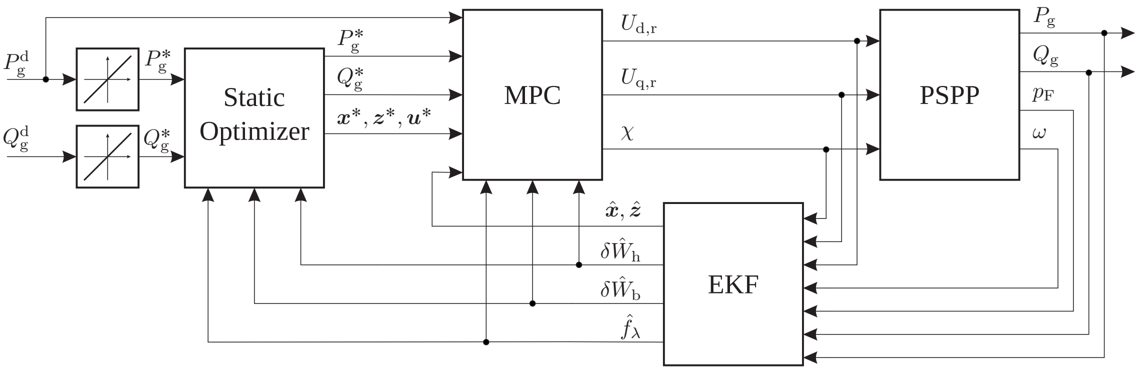

Fig. 4. Block diagram of the overall control strategy comprising the static optimizer, the model predictive control (MPC), the observer (EKF) and the model of the pumped storage power plant (PSPP).

water at the beginning of the first pipe $P_{h,t}$ and at the outlet of the sixth pipe $P_{h,b}$, i.e. $P_{in} = P_{h,t} - P_{h,b}$, with

$$P_{h,t} = \big(p_{1,1} + \rho g y_1(0)\big) q_{1,1} + \frac{\rho}{2}\big(q_{1,1}/A_1(0)\big)^2 q_{1,1} \quad (32a)$$

$$P_{h,b} = \big(p_{6,J_6} + \rho g y_6(L_6)\big) q_{6,J_6} + \frac{\rho}{2}\big(q_{6,J_6}/A_6(L_6)\big)^2 q_{6,J_6}. \quad (32b)$$

The output power $P_{out} = P_g$ coincides with the active grid output power. The pressure values in the definition of P_{in} can be easily expressed in terms of the piezometric heights $h_{1,1}$ and h_{6,J_6}, see (1). Moreover, the active and reactive grid output powers P_g and Q_g are defined in (22a) and (22b), respectively. Using (23) and (24), they can be expressed in terms of $I_{d,s}$, $I_{q,s}$ and $I_{d,t}$.

Remark 2: The optimal operating points are, as a matter of fact, also influenced by the system parameters. While the electrical and the geometric parameters of the PSPP are well known, parameters of the hydraulic part are afflicted with larger uncertainties. In particular, the pipe friction parameter f_λ and the turbine characteristic maps W_b, W_h might not be accurately known. Since they have an important influence on the optimal operating points, they have to be estimated in real operation. The estimated value $\hat{f}_\lambda$ of the pipe friction parameter and the estimated perturbations $\delta\hat{W}_b$, $\delta\hat{W}_h$ are utilized both in the MPC and the static optimizer.

B. Model Predictive Control

The starting point for the development of the MPC is the description of the system dynamics in the form

$$\dot{\boldsymbol{x}}(t) = \boldsymbol{f}(\boldsymbol{x}(t), \boldsymbol{z}(t), \boldsymbol{u}(t)), \quad (33a)$$

$$\dot{\boldsymbol{u}}(t) = \boldsymbol{v}(t), \quad (33b)$$

$$\boldsymbol{0} = \boldsymbol{g}(\boldsymbol{x}(t), \boldsymbol{z}(t), \boldsymbol{u}(t)). \quad (33c)$$

In this formulation, the system (30) is augmented by

$$\dot{U}_{d,r}(t) = v_{U_{d,r}}(t), \quad \dot{U}_{q,r}(t) = v_{U_{q,r}}(t), \quad \dot{\chi}(t) = v_\chi(t), \quad (33d)$$

which helps to increase the smoothness of the system's solutions and allows to take into account slew rate limits of the control input χ. Here, $\boldsymbol{v} = [v_{U_{d,r}}, v_{U_{q,r}}, v_\chi]^T$ denotes the new (virtual) control input utilized in the MPC.

The proposed MPC strategy is based on a direct transcription (full discretization) method [11], [12]. Let T_{mpc} denote the sampling time of the MPC. The prediction horizon $[nT_{mpc}, nT_{mpc} + T_{ph}]$ at the time step $t = nT_{mpc}$, $n \in \mathbb{N}_0$, is discretized in the form

$$0 = \tau_0 < \tau_1 < \ldots < \tau_{K-1} < \tau_K = T_{ph}, \quad (34)$$

where $K + 1$ is the number of grid points and T_{ph} denotes the prediction horizon length of the MPC. The vector

$$\boldsymbol{X}_{mpc,n}^T = \big[\boldsymbol{X}_{n|0}^T, \boldsymbol{X}_{n|1}^T, \ldots, \boldsymbol{X}_{n|K-1}^T, \boldsymbol{X}_{n|K}^T\big], \quad (35)$$

with $\boldsymbol{X}_{n|k}^T = [\boldsymbol{x}_{n|k}^T, \boldsymbol{z}_{n|k}^T, \boldsymbol{u}_{n|k}^T, \boldsymbol{v}_{n|k}^T]$ summarizes the predicted state and algebraic variables, and the predicted control and virtual control inputs at $t = nT_{mpc} + \tau_k$.

The implicit Euler method is employed for the temporal discretization of (33)[3]. Consequently, $\boldsymbol{x}_{n|k}$, $\boldsymbol{z}_{n|k}$, $\boldsymbol{u}_{n|k}$, and $\boldsymbol{v}_{n|k}$ are subject to the constraints

$$\boldsymbol{0} = \boldsymbol{x}_{n|k+1} - \boldsymbol{x}_{n|k} - \Delta\tau_k \boldsymbol{f}(\boldsymbol{x}_{n|k+1}, \boldsymbol{z}_{n|k+1}, \boldsymbol{v}_{n|k+1}), \quad (36a)$$

$$\boldsymbol{0} = \boldsymbol{u}_{n|k+1} - \boldsymbol{u}_{n|k} - \Delta\tau_k \boldsymbol{v}_{n|k+1}, \quad (36b)$$

$$\boldsymbol{0} = \boldsymbol{g}(\boldsymbol{x}_{n|k+1}, \boldsymbol{z}_{n|k+1}, \boldsymbol{u}_{n|k+1}), \quad (36c)$$

where $\Delta\tau_k = \tau_{k+1} - \tau_k$ denotes the local time step size with $k = 0, \ldots, K-1$. The predicted states and control inputs are initialized in the form

$$\boldsymbol{x}_{n|0} = \boldsymbol{x}_n, \quad \boldsymbol{z}_{n|0} = \boldsymbol{z}_n, \quad \boldsymbol{u}_{n|0} = \boldsymbol{u}_n^-, \quad \boldsymbol{v}_{n|0} = \boldsymbol{v}_n^-. \quad (37)$$

Here, $\boldsymbol{x}_n$ and $\boldsymbol{z}_n$ are the state and algebraic variables at $t = nT_{mpc}$, and $\boldsymbol{u}_n^-$ and $\boldsymbol{v}_n^-$ correspond to the optimal values, which where obtained in the preceding MPC iteration[4].

[3]The authors also studied other discretization methods with higher numeric accuracy as, e.g., the trapezoidal rule, the Hermite-Simpson method [11] and the Legendre-Gauss-Lobatto pseudospectral method [28], [29]. For the considered application in the NMPC, however, the implicit Euler method proved to be the best compromise between control accuracy and calculation times.

[4]Since not all state and algebraic variables can be measured, they will be replaced by their estimated values $\hat{\boldsymbol{x}}_n$ and $\hat{\boldsymbol{z}}_n$ obtained by the EKF described in Section IV-C.

Post-print version of the article: J. Mennemann, L. Marko, J. Schmidt, W. Kemmetmüller, and A. Kugi, "Nonlinear model predictive control of a variable-speed pumped-storage power plant," *IEEE Transactions on Control Systems Technology*, vol. 29, no. 2, pp. 645–660, 2021. DOI: 10.1109/TCST.2019.2956910
The content of this post-print version is identical to the published paper but without the publisher's final layout or copy editing.

The cost function $\mathcal{J}_n$ at time $t = nT_{\mathrm{mpc}}$ is defined as

$$\begin{aligned}\mathcal{J}_n &= w_1\mathcal{J}^{\mathrm{d}}_{P_{\mathrm{g}},n} + w_2\mathcal{J}^{\mathrm{d}}_{Q_{\mathrm{g}},n} + w_3\mathcal{J}^{\mathrm{d}}_{\chi,n} + w_4\mathcal{J}^{\mathrm{d}}_{\omega,n}\\ &\quad + w_5\mathcal{J}^{\mathrm{ub}}_{U_{\mathrm{r}},n} + w_6\mathcal{J}^{\mathrm{ub}}_{I_{\mathrm{r}},n} + w_7(\mathcal{J}^{\mathrm{lb}}_{P_{\mathrm{r}},n} + \mathcal{J}^{\mathrm{ub}}_{P_{\mathrm{r}},n})\\ &\quad + w_8(\mathcal{J}^{\mathrm{lb}}_{\chi,n} + \mathcal{J}^{\mathrm{ub}}_{\chi,n}) + w_9(\mathcal{J}^{\mathrm{lb}}_{v_\chi,n} + \mathcal{J}^{\mathrm{ub}}_{v_\chi,n})\\ &\quad + w_{10}(\mathcal{J}^{\mathrm{lb}}_{\boldsymbol{h},n} + \mathcal{J}^{\mathrm{ub}}_{\boldsymbol{h},n}) + w_{11}\mathcal{J}^{\mathrm{r}}_{\chi,n} + w_{12,n}\mathcal{J}^{\mathrm{r}}_{P_{\mathrm{g}},n}\end{aligned} \tag{38}$$

with the positive weights $w_1, \dots, w_{12,n}$. The first four parts of the cost function in (38) read as

$$\mathcal{J}^{\mathrm{d}}_{P_{\mathrm{g}},n} = \sum_{k=1}^{K} \gamma_{1,k}\Delta\tau_{k-1}(P_{\mathrm{g},n|k} - P^*_{\mathrm{g},n})^2, \tag{39a}$$

$$\mathcal{J}^{\mathrm{d}}_{Q_{\mathrm{g}},n} = \sum_{k=1}^{K} \gamma_{1,k}\Delta\tau_{k-1}(Q_{\mathrm{g},n|k} - Q^*_{\mathrm{g},n})^2, \tag{39b}$$

$$\mathcal{J}^{\mathrm{d}}_{\chi,n} = \sum_{k=1}^{K} \gamma_{1,k}\Delta\tau_{k-1}(\chi_{n|k} - \chi^*_n)^2, \tag{39c}$$

$$\mathcal{J}^{\mathrm{d}}_{\omega,n} = \sum_{k=1}^{K} \gamma_{1,k}\Delta\tau_{k-1}(\omega_{n|k} - \omega^*_n)^2, \tag{39d}$$

where the active and the reactive grid output power $P_{\mathrm{g},n|k}$ and $Q_{\mathrm{g},n|k}$ are defined by (22a), (22b), and are expressed in terms of the variables collected in (35). These parts of the cost function penalize deviations from the optimal stationary set point $P^*_{\mathrm{g},n}$, $Q^*_{\mathrm{g},n}$, χ^*_n, ω^*_n provided by the static optimizer of Section IV-A. As discussed before, static optimality is desired but is too restrictive at the beginning of the prediction horizon for fast changing set points. To take this into account, the monotonically increasing weights $\gamma_{1,k}$ are defined by means of a raised cosine function $\gamma_{1,k} = (1 - \cos(\pi\tau_k/T_{\mathrm{ph}}))/2$. Utilizing $\gamma_{1,k}$ in (39), the weight of the desired set point increases gradually towards the end of the prediction horizon, which helps to regularize the resulting optimal control problem.

Lower and upper bounds of scalar system variables are considered in form of the penalty functions

$$\mathcal{J}^{\mathrm{lb}}_{\xi,n} = \sum_{k=1}^{K} \Delta\tau_{k-1}(\min(\xi_{n|k} - \xi^{\mathrm{lb}}, 0))^2, \tag{40a}$$

$$\mathcal{J}^{\mathrm{ub}}_{\xi,n} = \sum_{k=1}^{K} \Delta\tau_{k-1}(\max(\xi_{n|k} - \xi^{\mathrm{ub}}, 0))^2, \tag{40b}$$

where $\xi \in \{U_{\mathrm{r}}, I_{\mathrm{r}}, P_{\mathrm{r}}, \chi, v_\chi\}$. The constraints on the pressure along the pipeline system are implemented in a similar way by

$$\mathcal{J}^{\mathrm{lb}}_{\boldsymbol{h},n} = \mathcal{J}^{\mathrm{lb}}_{\boldsymbol{h}_1,n} + \mathcal{J}^{\mathrm{lb}}_{\boldsymbol{h}_2,n} + \mathcal{J}^{\mathrm{lb}}_{\boldsymbol{h}_4,n} + \mathcal{J}^{\mathrm{lb}}_{\boldsymbol{h}_6,n} \tag{41a}$$

$$\mathcal{J}^{\mathrm{ub}}_{\boldsymbol{h},n} = \mathcal{J}^{\mathrm{ub}}_{\boldsymbol{h}_1,n} + \mathcal{J}^{\mathrm{ub}}_{\boldsymbol{h}_2,n} + \mathcal{J}^{\mathrm{ub}}_{\boldsymbol{h}_4,n} + \mathcal{J}^{\mathrm{ub}}_{\boldsymbol{h}_6,n}, \tag{41b}$$

with

$$\mathcal{J}^{\mathrm{lb}}_{\boldsymbol{h}_i,n} = \sum_{k=1}^{K}\sum_{j=1}^{J_i}(\min(h_{i,j,n|k} - h^{\mathrm{lb}}_{i,j}, 0))^2, \tag{42a}$$

$$\mathcal{J}^{\mathrm{ub}}_{\boldsymbol{h}_i,n} = \sum_{k=1}^{K}\sum_{j=1}^{J_i}(\max(h_{i,j,n|k} - h^{\mathrm{ub}}_{i,j}, 0))^2. \tag{42b}$$

Here, $h_{i,j,n|k}$ describes the piezometric height at the jth spatial grid point of the ith pipeline at time $nT_{\mathrm{mpc}} + \tau_k$.

The term

$$\mathcal{J}^{\mathrm{r}}_{\chi,n} = \sum_{k=1}^{K} \Delta\tau_{k-1}(v_{\chi,n|k} - v_{\chi,n|k-1})^2 \tag{43}$$

of the cost function (38) is used to penalize (abrupt) changes of the guide vane position.

A specific requirement for the operation of the PSPP is that (large) changes of the active grid output power should be realized in a monotonically increasing (or decreasing) way. This requirement results from the fact that a decrease in the active grid output power in the case when an increase is demanded can cause stability problems in the power grid. To account for this requirement, the term

$$\mathcal{J}^{\mathrm{r}}_{P_{\mathrm{g}},n} = \sum_{k=1}^{K} \Delta\tau_{k-1}\gamma_{2,k}(\dot{P}_{\mathrm{g},n|k} - \dot{P}_{\mathrm{g},n-1|1})^2 \tag{44}$$

is included in the cost function, where

$$\dot{P}_{\mathrm{g},n|k} = \frac{P_{\mathrm{g},n|k} - P_{\mathrm{g},n|k-1}}{\Delta\tau_{k-1}} \tag{45}$$

denotes the discrete time derivative of $P_{\mathrm{g},n|k}$ at $t = nT_{\mathrm{mpc}} + \tau_k$. By means of this term of the cost function, the slope of the output power $\dot{P}_{\mathrm{g},n|k}$ is forced to be similar to the slope of the output power at the beginning of the previous solution $\dot{P}_{\mathrm{g},n-1|1}$. In fact, (44) should not affect the whole trajectory of P_{g} in the prediction horizon since this would be too restrictive for the possible solutions of the optimal control problem. Thus, the gradually decreasing weight $\gamma_{2,k} = (1 + \cos(\pi\tau_k/T_{\mathrm{ph}}))/2$ is utilized, which implies that this term is inactive at the end of the prediction horizon. The term (44) of the cost function, however, does not make sense in situations when P_{g} is close to its desired value $P^{\mathrm{d}}_{\mathrm{g}}$. In this situation, any change to a higher or lower value would be penalized which would result in a rather slow reaction of the system. Simulation studies showed that utilizing the time dependent weighting

$$w_{12,n} = \max\left(0, \frac{|P^{\mathrm{d}}_{\mathrm{g},n} - P_{\mathrm{g},n}| - \Delta P_{\mathrm{g},w}}{P_{\mathrm{g},w}}\right)^{3/2}, \tag{46}$$

with constant parameters $\Delta P_{\mathrm{g},w}$ and $P_{\mathrm{g},w}$, circumvents this problem and gives good results for all operating conditions of the PSPP. It will be shown in Section VI that the resulting trajectories of P_{g} are in fact in very good agreement with the discussed monotonicity requirements. The constant weights $w_1, \dots, w_{11}$ and the parameters $\Delta P_{\mathrm{g},w}$ and $P_{\mathrm{g},w}$ are chosen in simulation studies and their values are summarized in Appendix B.

Based on this preparatory discussion, the optimal control problem to be solved iteratively by the MPC can be formulated as

$$\min_{\boldsymbol{X}_{\mathrm{mpc},n}} \mathcal{J}_n(\boldsymbol{X}_{\mathrm{mpc},n}) \tag{47}$$

subject to the equality constraints (36), (37), the cost function (38) with (39)-(46) and the vector of unknowns (35). Details of the efficient numeric solution of this optimal control problem will be discussed in Section V.

Post-print version of the article: J. Mennemann, L. Marko, J. Schmidt, W. Kemmetmüller, and A. Kugi, "Nonlinear model predictive control of a variable-speed pumped-storage power plant," *IEEE Transactions on Control Systems Technology*, vol. 29, no. 2, pp. 645–660, 2021. DOI: 10.1109/TCST.2019.2956910
The content of this post-print version is identical to the published paper but without the publisher's final layout or copy editing.

C. Extended Kalman Filter

Knowledge of the state and algebraic variables $\boldsymbol{x}$ and $\boldsymbol{z}$, respectively, is required in the MPC, cf. (37). In the real application only a few sensors are available. In particular, the distributed pressures and volume flows in the pipeline system are not accessible to measurements. Thus, a (nonlinear) observer will be utilized for the estimation of the states from the measured output. The observer is based on the model presented in Section III. This model, however, includes parameters which are not accurately known: (i) Pipe friction (represented by the Darcy-Weisbach friction coefficient f_λ) is influenced by many factors, e.g., surface roughness, fluid parameters, etc., and is therefore difficult to be accurately modeled. It is an important parameter of the model, in particular for the static optimizer. Thus, an estimation $\hat{f}_\lambda$ of f_λ has to be obtained by the observer. (ii) Another important model uncertainty is due to the characteristic maps W_b and W_h of the turbines, which can show significant deviations from the nominal behavior during long-term operation, e.g., due to wear. Thus, it is assumed that the real characteristic maps can be formulated as $W_\mathrm{b} = W_\mathrm{b}^\mathrm{n} + \delta W_\mathrm{b}$, $W_\mathrm{h} = W_\mathrm{h}^\mathrm{n} + \delta W_\mathrm{h}$, where W_b^n and W_h^n are the nominal characteristic maps and δW_b, δW_h are deviations, which have to be estimated by the EKF. To take into account these uncertainties in the observer design, the system model (30) is extended by the disturbance models

$$\frac{\mathrm{d}}{\mathrm{d}t}\delta W_\mathrm{b} = 0, \qquad \frac{\mathrm{d}}{\mathrm{d}t}\delta W_\mathrm{h} = 0, \qquad \frac{\mathrm{d}}{\mathrm{d}t} f_\lambda = 0, \tag{48}$$

which result from the assumption of unknown but constant (slowly varying) parameters.

For the derivation of the observer, the system (30a), (30b) and the disturbance model (48) are discretized in time by applying the implicit Euler method with a sampling time T_ekf. This yields the time-discrete model of the form[5]

$$\begin{aligned}
\mathbf{0} &= \boldsymbol{x}_{\ell+1} - \boldsymbol{x}_\ell - T_\mathrm{ekf}\,\tilde{\boldsymbol{f}}\big(\boldsymbol{x}_{\ell+1}, \boldsymbol{z}_{\ell+1}, \boldsymbol{u}_{\ell+1}, \\
&\qquad\qquad \delta W_{\mathrm{b},\ell+1}, \delta W_{\mathrm{h},\ell+1}, f_{\lambda,\ell+1}\big), && \text{(49a)}\\
\mathbf{0} &= \tilde{\boldsymbol{g}}\big(\boldsymbol{x}_{\ell+1}, \boldsymbol{z}_{\ell+1}, \boldsymbol{u}_{\ell+1}, \delta W_{\mathrm{b},\ell+1}, \delta W_{\mathrm{h},\ell+1}, f_{\lambda,\ell+1}\big), && \text{(49b)}\\
0 &= \delta W_{\mathrm{b},\ell+1} - \delta W_{\mathrm{b},\ell}, && \text{(49c)}\\
0 &= \delta W_{\mathrm{h},\ell+1} - \delta W_{\mathrm{h},\ell}, && \text{(49d)}\\
0 &= f_{\lambda,\ell+1} - f_{\lambda,\ell}, && \text{(49e)}
\end{aligned}$$

where $\tilde{\boldsymbol{f}}$ and $\tilde{\boldsymbol{g}}$ correspond to the right hand sides of (30a) and (30b) with W_h and W_b replaced by $W_\mathrm{h}^\mathrm{n}+\delta W_\mathrm{h}$ and $W_\mathrm{b}^\mathrm{n}+\delta W_\mathrm{b}$, respectively. The (future) control inputs $\boldsymbol{u}_{\ell+1}$ are provided by the MPC. The measured output $\boldsymbol{y}_\ell$ is given by

$$\boldsymbol{y}_\ell = \left[h_{2,J_2,\ell}, \omega_\ell, P_{\mathrm{g},\ell}, Q_{\mathrm{g},\ell}\right]^T, \tag{50}$$

and comprises the piezometric height h_{2,J_2} in front of the turbine (or equivalently the pressure p_F), the rotational speed ω of the turbine, and the active and reactive grid power P_g and Q_g.

[5]The sampling time T_ekf of the observer is not necessarily equal to the sampling time T_mpc of the MPC. It will be seen later that a faster sampling time for the observer is required to ensure an accurate estimation of the system states. To distinguish between these two sampling times $\boldsymbol{x}_n$ is utilized to denote the value of $\boldsymbol{x}$ at $t = nT_\mathrm{mpc}$ and $\boldsymbol{x}_\ell$ describes $\boldsymbol{x}$ at the time $t = \ell T_\mathrm{ekf}$.

The observer design for systems comprising long hydraulic pipelines was studied in detail in [30]. It was shown that an Extended Kalman Filter (EKF) is the right choice in terms of precision, speed and robustness. Thus, an EKF will also be utilized in this work, where a similar formulation of the EKF as described in [31] will be pursued. In the first step, the state $\boldsymbol{\xi}_\ell$ to be estimated is defined as

$$\boldsymbol{\xi}_\ell^T = \left[\boldsymbol{x}_\ell^T, \boldsymbol{z}_\ell^T, \delta W_{\mathrm{b},\ell}, \delta W_{\mathrm{h},\ell}, f_{\lambda,\ell}\right]. \tag{51}$$

Furthermore, let $\boldsymbol{\xi}_{\ell+1} = \boldsymbol{F}(\boldsymbol{\xi}_\ell, \boldsymbol{u}_{\ell+1})$ denote the (numerical) solution of (49). Then, the system dynamics for the EKF can be formulated as

$$\begin{aligned}
\boldsymbol{\xi}_{\ell+1} &= \boldsymbol{F}(\boldsymbol{\xi}_\ell, \boldsymbol{u}_{\ell+1}) + \boldsymbol{w}_\ell && \text{(52a)}\\
\boldsymbol{y}_\ell &= \boldsymbol{C}\boldsymbol{\xi}_\ell + \boldsymbol{v}_\ell, && \text{(52b)}
\end{aligned}$$

with the output matrix $\boldsymbol{C}$. Here it is assumed that the system dynamics is perturbed by the zero-mean process noise $\boldsymbol{w}_\ell$ with covariance matrix $\hat{\boldsymbol{Q}} > 0$ and the measured output is distorted by the zero-mean measurement noise $\boldsymbol{v}_\ell$ with covariance matrix $\hat{\boldsymbol{R}} > 0$.

The EKF is implemented similar as described in [30], [31] and thus not repeated here. The values of $\hat{\boldsymbol{Q}}$ and $\hat{\boldsymbol{R}}$ are obtained from data of the utilized sensors and by tuning of the EKF in simulations, see Appendix C.

V. Details of the Implementation

Fast sampling times T_mpc and T_ekf of the MPC and the EKF, respectively, are essential to obtain accurate tracking and estimation results. At the same time, the sampling times have to be large enough to allow for a calculation of the controller and observer equations in real time. Solving the optimization problem of the MPC is computationally complex and can be obtained in reasonable time only by utilizing state-of-the-art hardware. The results and calculation times reported in this work correspond to an Ubuntu 18.04 operating system running on a workstation computer (i9-9980XE CPU, 32 GB RAM). $T_\mathrm{mpc} = 60\,\mathrm{ms}$ was obtained in simulation studies as a suitable sampling time for the MPC where a real-time solution of the underlying optimization problem can be guaranteed. Faster sampling times are meaningful for the EKF to obtain a high estimation accuracy. In our case, $T_\mathrm{ekf} = 12\,\mathrm{ms}$ was chosen. Finally, a prediction horizon of $T_\mathrm{ph} = 5\,\mathrm{s}$ gives a good compromise between control performance and computational costs.

Due to the computation time required to solve the MPC problem, the solution is lagging behind real time by the sampling time T_mpc. To approximately compensate for this dead time and to account for the different sampling times of the MPC, the EKF and the (simulated) system model, a linear interpolation of the optimal virtual control inputs (i.e. the time derivatives of the real control inputs) of the MPC is performed. This interpolation process is illustrated in Fig. 5 with v_mpc representing one of the virtual control inputs $v_{U_\mathrm{d,r}}$, $v_{U_\mathrm{q,r}}$ or v_χ. This figure shows that the optimal virtual control inputs at the times $t = (n+1)T_\mathrm{mpc} + mT_\mathrm{ekf}$, $m = 1, \ldots, 5$, are obtained by interpolation of the virtual control inputs $\boldsymbol{v}_{n|0}$ and $\boldsymbol{v}_{n|1}$ of the MPC.

Post-print version of the article: J. Mennemann, L. Marko, J. Schmidt, W. Kemmetmüller, and A. Kugi, “Nonlinear model predictive control of a variable-speed pumped-storage power plant,” *IEEE Transactions on Control Systems Technology*, vol. 29, no. 2, pp. 645–660, 2021. DOI: 10.1109/TCST.2019.2956910
The content of this post-print version is identical to the published paper but without the publisher’s final layout or copy editing.

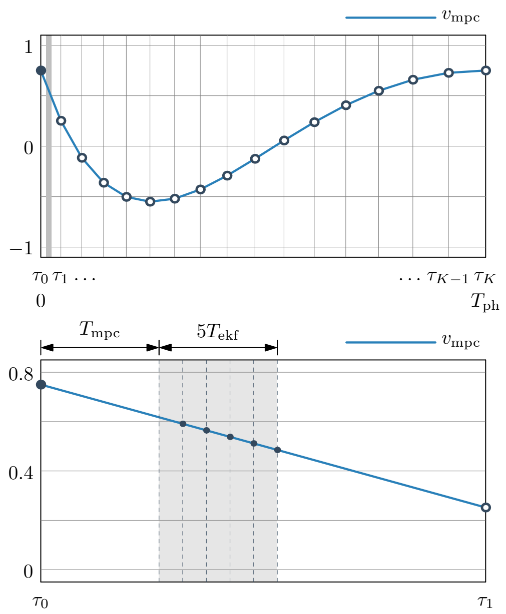

Fig. 5. Linear interpolation of v_{mpc} representing one of the virtual control inputs $v_{U_{\mathrm{d,r}}}$, $v_{U_{\mathrm{q,r}}}$ or v_{χ}. The evaluation takes place with a constant time delay of T_{mpc}.

The real control inputs of the EKF are calculated in the form

$$U_{\mathrm{d,r},\ell+1} = U_{\mathrm{d,r},\ell} + T_{\mathrm{ekf}}\, v_{U_{\mathrm{d,r},m}}, \tag{53a}$$
$$U_{\mathrm{q,r},\ell+1} = U_{\mathrm{q,r},\ell} + T_{\mathrm{ekf}}\, v_{U_{\mathrm{q,r},m}}, \tag{53b}$$
$$\chi_{\ell+1} = \chi_{\ell} + T_{\mathrm{ekf}}\, v_{\chi,m}, \tag{53c}$$

where $v_{U_{\mathrm{d,r},m}}$, $v_{U_{\mathrm{q,r},m}}$, $v_{\chi,m}$ are the interpolated virtual control inputs and ℓ is the global index of the EKF, which is increased after each application of (53) for the local index $m = 1, \ldots, 5$. A similar interpolation approach will be utilized to obtain the control inputs applied to the (simulated) pumped storage power plant.

Remark 3: Instead of interpolating the virtual control inputs, one may interpolate the real control inputs, which are also part of the solution of the MPC. The chosen approach, however, guarantees smoother control inputs, which is helpful to avoid oscillations of the closed-loop system in case of rapidly changing operating points.

The numerical algorithms are implemented in MATLAB R2017A, where the MATLAB plugin of CASADI 3.4 is utilized as an efficient way to implement and solve the optimization problems of the MPC and the static optimizer. CASADI is an open-source tool for nonlinear optimization and algorithmic differentiation [32], [33]. By means of CASADI it is easily possible to provide all relevant derivative information (e.g., the Jacobian or Hessian of the constraints or cost function) needed to efficiently solve a nonlinear optimization problem. CASADI also includes a set of proven solvers. In this work, IPOPT [34] is used, which is an open-source implementation of the interior point method and is capable of solving large-scale nonlinear optimization problems.

The times needed to solve nonlinear optimization problems of the MPC and the static optimizer must not exceed T_{mpc}. In the following, the measures which are taken to satisfy this requirement are described in more detail: (i) The solution and the Lagrange multipliers of the optimal control problem on the previous prediction horizon are utilized as an initial guess for the current prediction horizon. This only makes sense if the nonlinear optimization problems of two consecutive prediction horizons are sufficiently similar. This implies that the set point P_{g}^*, Q_{g}^* provided by the static optimizer is not allowed to change too abruptly. Thus, the rates of change $\dot{P}_{\mathrm{g}}^*$, $\dot{Q}_{\mathrm{g}}^*$ are limited by $\pm\dot{P}_{\mathrm{g}}^{\max}$, $\pm\dot{Q}_{\mathrm{g}}^{\max}$, respectively, by introducing a rate limiter in front of the static optimizer. In the real application, mostly the active power and a (constant) power factor $\cos(\varphi)$ are defined by the operator instead of specifying the reactive power. This implies that it is sufficient to limit $\dot{P}_{\mathrm{g}}^*$, since the reactive power is directly related to the active power by a (constant) factor. The choice of $\dot{P}_{\mathrm{g}}^{\max}$ has a strong influence on the solution of the MPC. If $\dot{P}_{\mathrm{g}}^{\max}$ is chosen too high, the solution of the optimization problem on the previous prediction horizon is not a good initialization for the current prediction horizon. This poor initial guess brings along that more iterations are necessary to solve the underlying nonlinear optimization problem, which may take longer than T_{mpc}. If, on the other hand, $\dot{P}_{\mathrm{g}}^{\max}$ is chosen too small, the control performance with respect to set point changes is deteriorated. In the simulations of Section VI, $\dot{P}_{\mathrm{g}}^{\max} = 55\,\mathrm{MW/s}$ is chosen, which constitutes a good compromise between closed-loop performance and computational costs for solving the optimization problem. This value is also considerably larger than the reaction speed typically demanded by grid operators.

(ii) Another important point for a fast solution of the MPC is to minimize the number of temporal discretization points τ_k, $k = 0, \ldots, K$, cf. (34). This can be achieved by a non-uniform discretization in time. In the proposed implementation, $K = 16$ gradually increasing time intervals $\Delta\tau_k = \tau_{k+1} - \tau_k$ are employed, which are defined by $\Delta\tau_k = \eta\,\Delta\tau_{k-1}$, $\tau_k = \tau_{k-1} + \Delta\tau_{k-1}$, with $\tau_0 = 0$, $\Delta\tau_0 = T_{\mathrm{ph}}(1-\eta)/(1-\eta^K)$, $\eta = \zeta^{1/(K-1)}$ and $\zeta = 1.5$. This choice is based on the observation that the trajectories of the states and the control inputs tend to change more quickly at $\tau_0 = 0$ than at $\tau_K = T_{\mathrm{ph}}$. To obtain the same temporal resolution at τ_0 by means of a uniform temporal grid, approximately $K = 24$ time intervals would be required.

(iii) An efficient and accurate solution method for the DAE system (33) is essential for a fast solution of the underlying optimization problem. In this work, the implicit Euler method is utilized, which represents an excellent method in terms of numerical stability.

(iv) Finally, an important contribution to a fast solution of the optimization problems results from the realization of all lower and upper bounds by means of penalty functions. Of course, an implementation of the lower and upper bounds as (hard) inequality constraints is easily possible within the CASADI framework. It was, however, found in a number of numerical experiments that the solution times of this approach are about one order of magnitude larger than the times when

Post-print version of the article: J. Mennemann, L. Marko, J. Schmidt, W. Kemmetmüller, and A. Kugi, "Nonlinear model predictive control of a variable-speed pumped-storage power plant," *IEEE Transactions on Control Systems Technology*, vol. 29, no. 2, pp. 645–660, 2021. DOI: 10.1109/TCST.2019.2956910

using penalty functions.

Remark 4: Please note that the number of variables in the optimization problem of the static optimizer is very small in comparison to those in the MPC. Therefore, computing time is not a major issue for the static optimizer, which makes it possible to implement upper and lower bounds also as hard inequality constraints.

VI. Results

A. Simulation Model

For testing the control and observer strategy presented in Section IV, a simulation model is set up which utilizes the method of characteristics (MOC) to describe the dynamics of the hydraulic pipeline system. The MOC is the most common method for the simulation of pressure waves in hydraulic pipeline systems, see, e.g. [20]. The MOC is subject to a strict Courant-Friedrichs-Lewy (CFL) condition, which implies that the number of spatial grid points is determined by the local wave speeds and the time step size Δt. Simulation studies showed that $\Delta t = 4\,\mathrm{ms}$ is a suitable time step size for the simulation model. Given the system parameters, this results in $2 \times (211 + 8 + 14 + 257) = 980$ spatial grid points for the approximation of h_i and q_i, $i \in \{1, 2, 4, 6\}$. As a matter of fact, this a significantly higher number than the 52 dynamical states utilized in the spectral element approximation in Section III-A.

The remaining part of the simulation model coincides with the model used for the controller design, except for additional measurement noise and model uncertainties, which will be discussed subsequently. While the time propagation method of the hydraulic system is fixed by the MOC, the mechanical and electrical systems of the simulation model are numerically integrated by the implicit Euler method.

As discussed before, significant differences can be expected for certain model parameters between the nominal model utilized in the controller and observer design and the real plant. In particular, the following parametric uncertainties are considered in the subsequent simulation studies: (i) The effective wave speed c in the pipelines is a function of the pipe stiffness and the compressibility of the water. Since both of them are not exactly known in real operation, the wave speeds of the simulation model are perturbed compared to the nominal wave speeds depicted in Fig. 3. In particular, the wave speeds of the first and second pipeline are increased by five percent and the wave speeds of the fourth and sixth pipeline are decreased by five percent. With this choice, the numerical solutions of the perturbed and unperturbed system will diverge significantly in the transient regime. (ii) It is assumed that only a rough estimate of the Darcy-Weisbach friction factor f_λ of (3) is known. This parameter is estimated by means of the EKF according to Section IV-C and only this estimated value $\hat{f}_\lambda$ is utilized in the control strategy. In the simulation model, a nominal value $f_\lambda = 0.0065$ is chosen. (iii) The most pronounced uncertainties are expected to occur in the model of the turbines, i.e. in the characteristic maps W_b and W_h. In general, it is difficult to accurately predict the change of the characteristic maps, e.g., due to wear. In order to approximately account for the uncertainties of the turbine in the simulation studies, the nominal values h_ref, q_ref, M_ref, and ω_ref of the simulation model are adjusted to $\tilde{h}_\mathrm{ref} = 1.0065\,h_\mathrm{ref}$, $\tilde{q}_\mathrm{ref} = 1.0065\,q_\mathrm{ref}$ and $\tilde{M}_\mathrm{ref} = M_\mathrm{ref} - 0.0065\,M_\mathrm{ref}$. This results in a reduction of the turbine efficiency of the simulation model by approximately two percent and changes the location of the operating point of maximum efficiency.

In the subsequent simulation studies, the measured quantities p_F (or equivalently h_{2,J_2}), ω, P_g, and Q_g are corrupted by measurement noise, whose parameters are summarized in Appendix C.

B. Simulations

In the numerical simulation scenario, different set point changes of the desired active and reactive grid output power P_g^d and Q_g^d, respectively, are considered, see Fig. 6 a). This figure shows that, despite the very demanding simulation scenario, the active and reactive grid output powers P_g and Q_g closely follow the reference values. Furthermore, it can be seen that changes of the active grid output power P_g evolve in the required monotonically increasing or decreasing way. This is achieved by the term (44) of the optimization problem of the MPC. Since no such restrictions have been set on the reactive grid output power, larger variations in the time evolution of Q_g can be observed. The corresponding time evolution of the control inputs is depicted in Fig. 6 b) and Fig. 6 c). Moreover, Fig. 6 d) shows that the lower and upper bounds of the adjustment speed v_χ of the guide vane position χ is active and kept well for large changes of the desired active power P_g^d.

The time evolutions of the angular velocity ω and the volume flow q_F through the Francis turbines are shown in Fig. 6 e) and Fig. 6 f), respectively. Please note that the changes in the angular velocity ω result from the changes in the optimal operating points for different desired active powers. Fig. 6 g) and Fig. 6 h) show the time evolutions of the absolute values of the rotor voltage and the rotor current, and the time evolution of the rotor power is depicted in Fig. 6 i). Again it should be noted that almost all bounds of the electric variables get active at several occasions during the simulation. In all cases, these inequality constraints are kept very well, although they are realized in form of penalty functions in the MPC.

A unique feature of the proposed optimal control strategy is that pressure bounds along the whole pipeline system are systematically taken into account. The first significant pressure variation occurs shortly after $t = 80\,\mathrm{s}$, i.e. shortly after a large step in the active grid power from $75\,\mathrm{MW}$ to $325\,\mathrm{MW}$ has been requested by the operator. The resulting pressure distributions on the fourth and sixth pressure line (cf. Fig. 2) are depicted in the upper row of Fig. 7 at three consecutive times[6] $t_1 = 80\,\mathrm{s}$, $t_2 = 81.7\,\mathrm{s}$ and $t_3 = 85.8\,\mathrm{s}$. Here, the results of two different simulations are compared: Fig. 7 a) corresponds to the scenario where w_{10} in (38) is set to zero, i.e. pressure bounds are not taken into account. These results clearly show that large violations of the pressure bounds occur

[6] The first and second pressure line show similar pressure fluctuations, however, the strongest variations appear on the fourth and sixth pipeline.

Post-print version of the article: J. Mennemann, L. Marko, J. Schmidt, W. Kemmetmüller, and A. Kugi, “Nonlinear model predictive control of a variable-speed pumped-storage power plant,” *IEEE Transactions on Control Systems Technology*, vol. 29, no. 2, pp. 645–660, 2021. DOI: 10.1109/TCST.2019.2956910
The content of this post-print version is identical to the published paper but without the publisher’s final layout or copy editing.

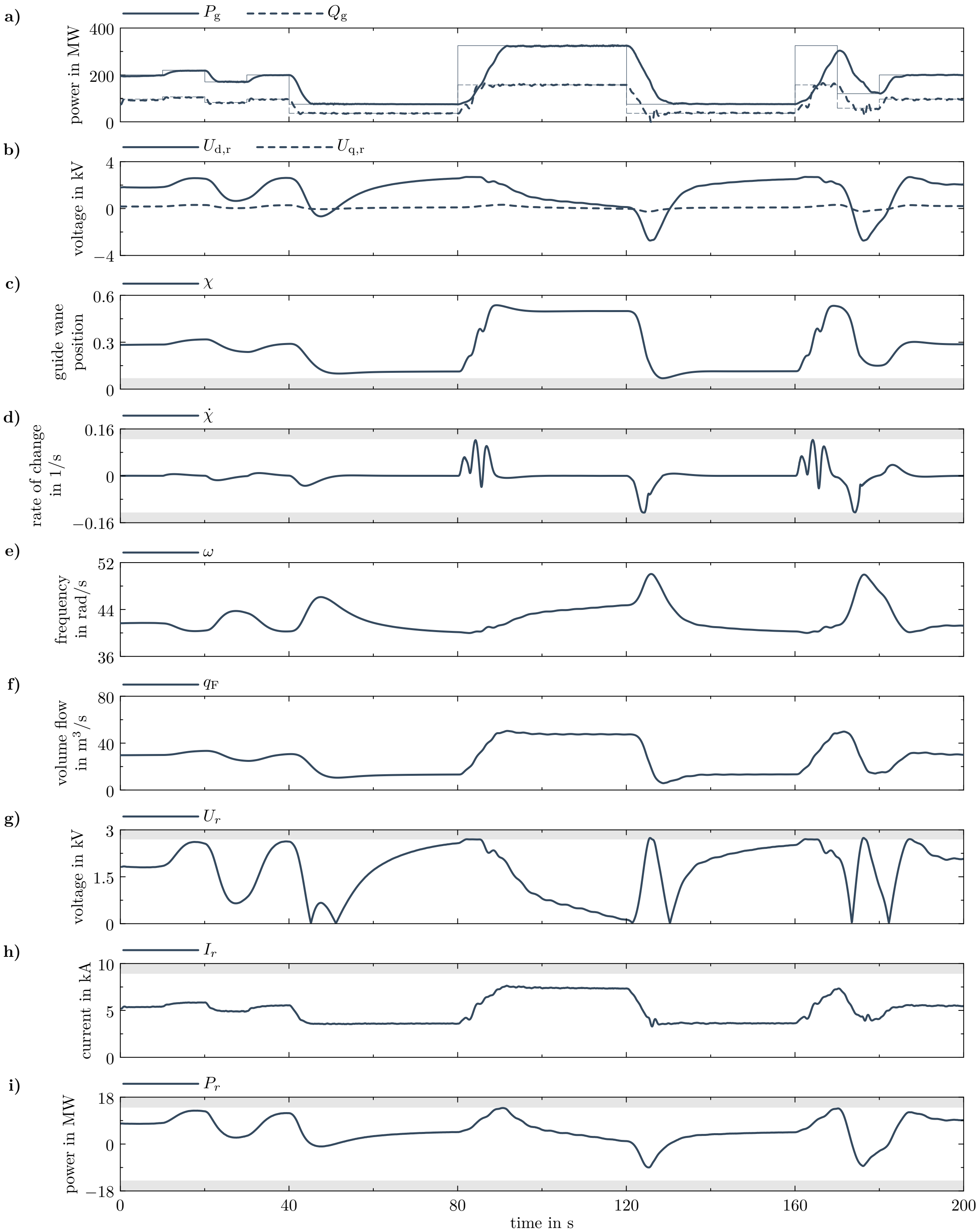

Fig. 6. Results of a comprehensive numerical simulation including very strong variations of the desired grid output powers (first part). Inadmissible values are shaded in gray.

Post-print version of the article: J. Mennemann, L. Marko, J. Schmidt, W. Kemmetmüller, and A. Kugi, "Nonlinear model predictive control of a variable-speed pumped-storage power plant," *IEEE Transactions on Control Systems Technology*, vol. 29, no. 2, pp. 645–660, 2021. DOI: 10.1109/TCST.2019.2956910
The content of this post-print version is identical to the published paper but without the publisher's final layout or copy editing.

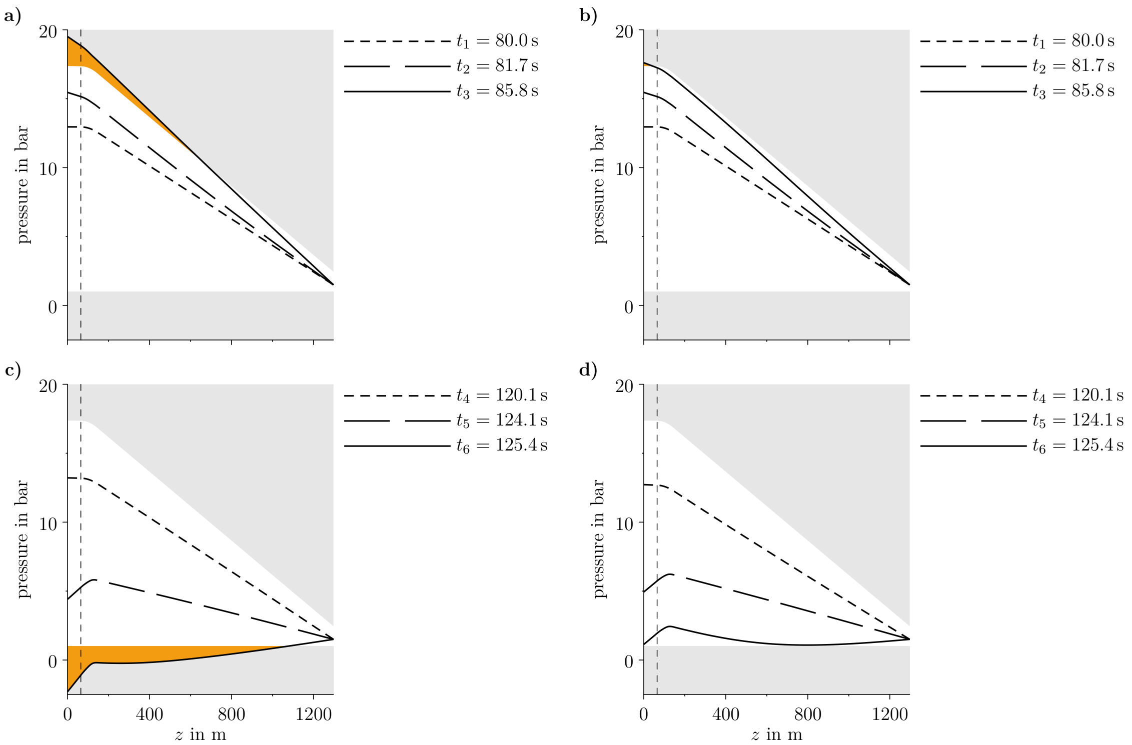

Fig. 7. Snapshots of the pressure distribution on the fourth and sixth pipeline at different times. The dashed vertical line indicates the end and the beginning of the fourth and sixth pressure line, respectively. Inadmissible values of the pressure are shaded in gray and violations are highlighted in orange. Left: Pressure bounds are neglected in the MPC. Right: Pressure bounds are taken into account in the MPC.

if they are ignored in the MPC. These violations can yield an increased wear and in the worst case even a damage of the pipelines. By means of the proposed MPC strategy, these violations can be efficiently avoided as can be seen from Fig. 7 b) corresponding to the scenario where pressure bounds are taken into account.

Similar results are obtained at $t = 120\,\mathrm{s}$, where the active grid output power is decreased from $325\,\mathrm{MW}$ to $75\,\mathrm{MW}$. The lower row of Fig. 7 depicts the pressure distributions at three consecutive times $t_4 = 120.1\,\mathrm{s}$, $t_5 = 124.1\,\mathrm{s}$ and $t_6 = 125.4\,\mathrm{s}$. Fig. 7 c) shows that the pressure in the pipeline can fall significantly below the minimum allowed value of $1\,\mathrm{bar}$. Below this pressure, water starts to evaporate and thus, cavitation can occur[7]. Cavitation is in particular harmful at the turbine and for the pipelines when the vapor bubbles collapse, since this may introduce a water hammer and thus damage the system. It is again shown that by systematically taking into account the pressure bounds in the MPC, cavitation can be circumvented, see Fig. 7 d). Furthermore, it should be emphasized that the pressure bounds are considered along the whole pipeline system and not only at the end points of the pressure lines.

The most pronounced pressure variations arise at the downstream side of the Francis turbines, i.e. at the beginning of the fourth and sixth pipeline, see Fig. 2. In Fig. 8 b), the time evolution of the pressure for both cases with and without taking into account the pressure bounds are depicted. Clearly, this plot shows that the pressure constraints are well satisfied in the proposed MPC strategy.

The proposed EKF includes an estimation of the unknown pipe friction parameter f_λ and the uncertainties δW_b and δW_h of the characteristic maps, cf. Section IV-C. The time evolution of these estimated parameters is shown in Fig. 8 c) and d). It can be seen that the estimated pipe friction parameter converges from its initial estimated value $\hat{f}_\lambda = 2f_\lambda$ to the parameter set in the simulated plant and thus gives meaningful estimates. A direct physical interpretation of the estimations $\delta\hat{W}_\mathrm{b}$, $\delta\hat{W}_\mathrm{h}$ is not possible. The results given in Fig. 8 prove that with these estimations the intended stationary accuracy of the controlled active and reactive power is achieved. Please note that without these estimated values, significant stationary deviations will occur.

Fig. 8 e) and Fig. 8 f) depict the computing times and the number of iterations needed to solve the nonlinear optimization problems of the MPC. Due to the initialization discussed in Section V, only two iterations are needed to solve the optimization problems of the MPC in cases when the desired active power is kept constant. As expected, more iterations (up to 4) are required, when large and abrupt changes of the desired grid output power are demanded. In all cases, the

[7]The negative values of the simulated pressure result from the simple fluid model, which does not include evaporation at low pressures. In a real system, evaporation of the fluid will limit the pressure to a physical minimum of $0\,\mathrm{bar}$.

Post-print version of the article: J. Mennemann, L. Marko, J. Schmidt, W. Kemmetmüller, and A. Kugi, “Nonlinear model predictive control of a variable-speed pumped-storage power plant,” *IEEE Transactions on Control Systems Technology*, vol. 29, no. 2, pp. 645–660, 2021. DOI: 10.1109/TCST.2019.2956910
The content of this post-print version is identical to the published paper but without the publisher’s final layout or copy editing.

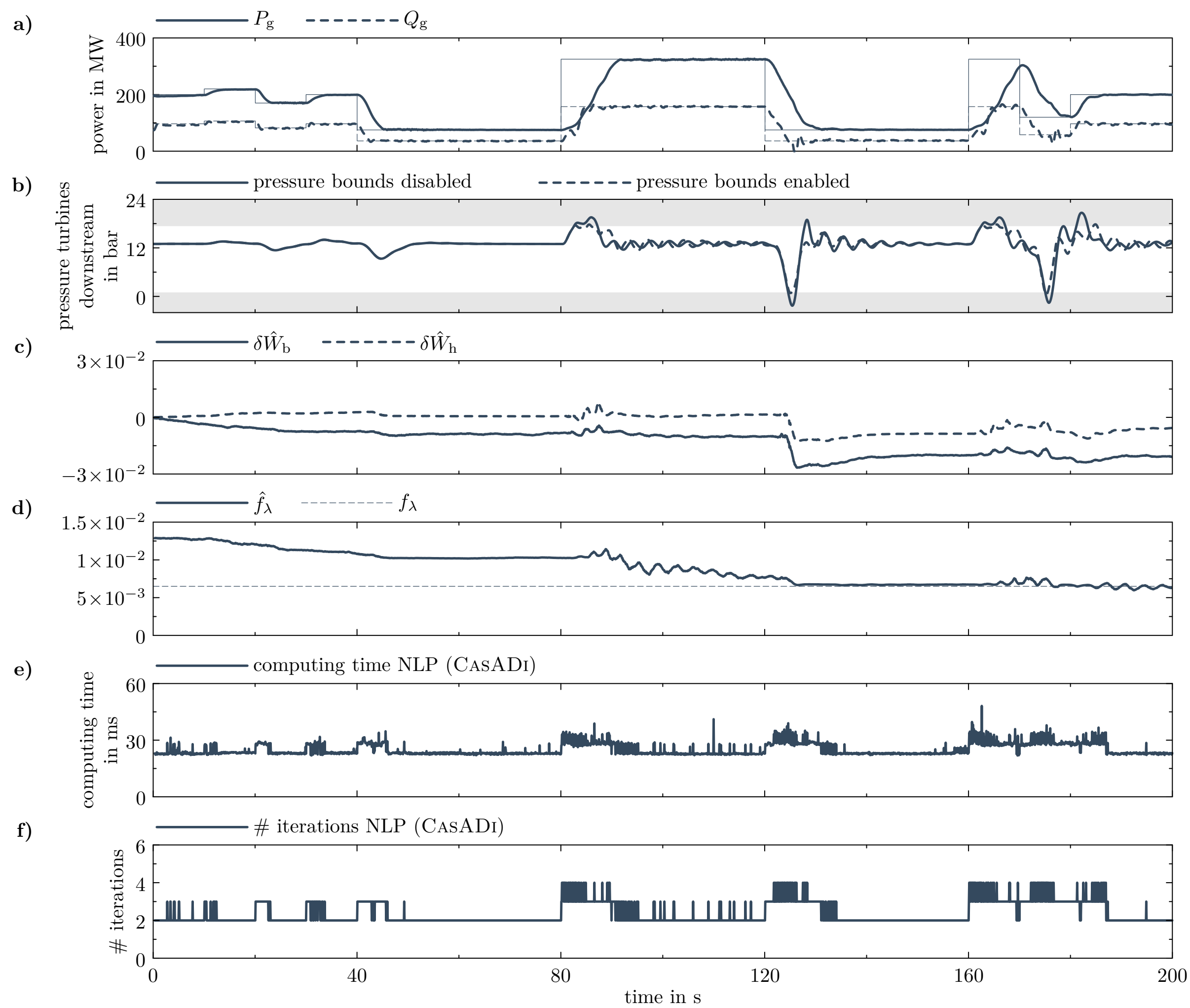

Fig. 8. Results of a comprehensive numerical simulation including very strong variations of the desired grid output powers (second part). Inadmissible values are shaded in gray.

required computing time is kept well below the maximum time[8] $T_{\mathrm{mpc}} = 60\,\mathrm{ms}$.

VII. Conclusions

In this paper, the optimal control of a variable-speed pumped storage power plant (PSPP) was considered. The goal was to ensure an optimal operation of the PSPP in the quasi-stationary case and to allow for highly dynamic set point changes in the desired active and reactive grid powers without violating any constraints. In particular, complying with the lower and upper limits of the pressure along the long pipelines is essential for a safe system operation.

The control concept presented in this paper comprises a static optimizer, a nonlinear model predictive controller (MPC) and an Extended Kalman Filter to estimate the unmeasurable state variables and some uncertain (slowly varying) parameters. A crucial point in the development of a real-time capable nonlinear MPC is the availability of a computationally efficient and accurate mathematical model which captures the essential dynamics and the main nonlinearities of the system. In this context, the application of the spectral element method to the spatial discretization of the hyperbolic PDEs of the long pipelines turns out to be a key step in deriving a numerically efficient low-dimensional but highly accurate mathematical model.

In the paper, a number of further measures were presented to be able to solve the underlying nonlinear optimization problems within a sampling time of $60\,\mathrm{ms}$. It could be demonstrated in simulation studies that the proposed control concept exhibits an excellent closed-loop performance even for large step changes in the desired grid power without violating any system constraints.

[8]A maximum number of 5 iterations can be calculated within $60\,\mathrm{ms}$. If no converged solution is obtained after 5 iterations, the previous optimal solution is extrapolated and the iteration is continued with the same desired value in the next sampling period.

Post-print version of the article: J. Mennemann, L. Marko, J. Schmidt, W. Kemmetmüller, and A. Kugi, "Nonlinear model predictive control of a variable-speed pumped-storage power plant," *IEEE Transactions on Control Systems Technology*, vol. 29, no. 2, pp. 645–660, 2021. doi: 10.1109/TCST.2019.2956910
The content of this post-print version is identical to the published paper but without the publisher's final layout or copy editing.

The physics-based modeling in combination with the model-based controller design also allows for an easy adaptation to different plant sizes and a transfer to other system topologies. In particular, the proposed control strategy can be easily transferred to variable speed power plants comprising a synchronous generator with a fully rated back-to-back converter. Thus, future research is directed towards the independent operation of two plant units and the extension to other system topologies, including synchronous machines with fully rated back-to-back converters or several plant units.

APPENDIX A
MATRICES OF THE ELECTRICAL SYSTEM

The matrices in (21) of Section III-B are given by [4]

$$\boldsymbol{A}_{\mathrm{D1}} = \frac{1}{\gamma}\begin{bmatrix} L_{\mathrm{r}}R_{\mathrm{s}} & \gamma\omega_{\mathrm{s}} & -L_{\mathrm{m}}R_{\mathrm{r}} & 0 \\ -\gamma\omega_{\mathrm{s}} & L_{\mathrm{r}}R_{\mathrm{s}} & 0 & L_{\mathrm{m}}R_{\mathrm{r}} \\ -L_{\mathrm{m}}R_{\mathrm{s}} & 0 & L_{\mathrm{s}}R_{\mathrm{r}} & \gamma\omega_{\mathrm{s}} \\ 0 & -L_{\mathrm{m}}R_{\mathrm{s}} & -\gamma\omega_{\mathrm{s}} & L_{\mathrm{s}}R_{\mathrm{r}} \end{bmatrix},$$

$$\boldsymbol{A}_{\mathrm{D2}} = \frac{p}{\gamma}\begin{bmatrix} 0 & -L_{\mathrm{m}}^2 & 0 & -L_{\mathrm{m}}L_{\mathrm{r}} \\ L_{\mathrm{m}}^2 & 0 & L_{\mathrm{m}}L_{\mathrm{r}} & 0 \\ 0 & L_{\mathrm{s}}L_{\mathrm{m}} & 0 & L_{\mathrm{r}}L_{\mathrm{s}} \\ -L_{\mathrm{s}}L_{\mathrm{m}} & 0 & -L_{\mathrm{r}}L_{\mathrm{s}} & 0 \end{bmatrix},$$

$$\boldsymbol{G}_{\mathrm{D}} = \frac{1}{\gamma}\begin{bmatrix} -L_{\mathrm{r}} & 0 & L_{\mathrm{m}} & 0 \\ 0 & -L_{\mathrm{r}} & 0 & L_{\mathrm{m}} \\ L_{\mathrm{m}} & 0 & -L_{\mathrm{s}} & 0 \\ 0 & L_{\mathrm{m}} & 0 & -L_{\mathrm{s}} \end{bmatrix},$$

where $\gamma = L_{\mathrm{m}}^2 - L_{\mathrm{r}}L_{\mathrm{s}}$.

APPENDIX B
WEIGHTS OF THE MPC

The weights in the cost function (38) are given by

$$\begin{array}{lll} w_1 = 2.2\times 10^{-17} & w_2 = 1.7\times 10^{-16} & w_3 = 2.5\times 10^{-3} \\ w_4 = 2\times 10^{-6} & w_5 = 1\times 10^{-5} & w_6 = 0 \\ w_7 = 1.5\times 10^{-15} & w_8 = 1\times 10^{4} & w_9 = 1\times 10^{2} \\ w_{10} = 1\times 10^{-2} & w_{11} = 5 & \end{array}$$

and $\Delta P_{\mathrm{g},w} = 2.5\,\mathrm{MW}$, $P_{\mathrm{g},w} = 250\,\mathrm{MW}$. Here, the weight w_6, which corresponds to the upper bound of I_{r}, is set to zero, since it is irrelevant in the considered system. Alternatively, the term $\mathcal{J}_{I_{\mathrm{r}}}^{\mathrm{ub}}$ in (38) could be removed. However, note that whether the upper bound of I_{r} is relevant or not strongly depends on the parameters of the electrical system.

APPENDIX C
PARAMETERS OF THE EKF

The covariance matrix $\hat{\boldsymbol{Q}}$ of the EKF in Section IV-C is chosen diagonal. The elements corresponding to the currents $\hat{I}_{\mathrm{d,s}}$, $\hat{I}_{\mathrm{q,s}}$, $\hat{I}_{\mathrm{d,r}}$, $\hat{I}_{\mathrm{q,r}}$ and $\hat{I}_{\mathrm{d,t}}$ are set to $1\times 10^{-2}\,\mathrm{A}^2$. The elements corresponding to $\delta\hat{W}_{\mathrm{b}}$, $\delta\hat{W}_{\mathrm{h}}$ and $\hat{f}_\lambda$ are given by 1.25×10^{-8}, 0.25×10^{-8} and 1.25×10^{-10}, respectively. All remaining values on the diagonal of $\hat{\boldsymbol{Q}}$ are set to 5×10^{-4}.

The measurement noise $\boldsymbol{v}_\ell$ in (52b) is modeled using white Gaussian noise characterized by the standard deviations $\sigma_{h_{2,J_2}} = 5\,\mathrm{m}$, $\sigma_\omega = 0.1\,\mathrm{rad/s}$ and $\sigma_{P_{\mathrm{g}}} = \sigma_{Q_{\mathrm{g}}} = 0.65\,\mathrm{MW}$. Accordingly, the covariance matrix is given by $\hat{\boldsymbol{R}} = \mathrm{diag}(\sigma_{h_{2,J_2}}^2, \sigma_\omega^2, \sigma_{P_{\mathrm{g}}}^2, \sigma_{Q_{\mathrm{g}}}^2)$.

ACKNOWLEDGMENT

The authors would like to thank Andritz Hydro GmbH for the financial support. In particular, they would like to thank M. Egretzberger and M. Meusburger of Andritz Hydro GmbH for the provided data of the PSPP and the helpful discussions. Furthermore, the financial support by the Christian Doppler Research Association, the Austrian Federal Ministry for Digital and Economic Affairs, and the National Foundation for Research, Technology and Development is gratefully acknowledged.

REFERENCES

[1] Y. M. Atwa and E. F. El-Saadany, “Optimal allocation of ESS in distribution systems with a high penetration of wind energy,” *IEEE Transactions on Power Systems*, vol. 25, no. 4, pp. 1815–1822, 2010.

[2] J. Perez, M. Chazarra, J. Garcia-Gonzalez, G. Cavazzini, and A. Stoppato, “Trends and challenges in the operation of pumped-storage hydropower plants,” *Renewable and Sustainable Energy Reviews*, vol. 44, pp. 767–784, 2015.

[3] Y. Pannatier, B. Kawkabani, C. Nicolet, J. J. Simond, A. Schwery, and P. Allenbach, “Investigation of control strategies for variable-speed pump-turbine units by using a simplified model of the converters,” *IEEE Transactions on Industrial Electronics*, vol. 57, no. 9, pp. 3039–3049, 2010.

[4] J. Schmidt, W. Kemmetmüller, and A. Kugi, “Modeling and static optimization of a variable speed pumped storage power plant,” *Renewable Energy*, vol. 111, pp. 38 – 51, 2017.

[5] J. Liang, X. Yuan, Y. Yuan, Z. Chen, and Y. Li, “Nonlinear dynamic analysis and robust controller design for Francis hydraulic turbine regulating system with a straight-tube surge tank,” *Mechanical Systems and Signal Processing*, vol. 85, pp. 927–946, 2017.

[6] Y. Xu, Y. Zheng, Y. Du, W. Yang, X. Peng, and C. Li, “Adaptive condition predictive-fuzzy PID optimal control of start-up process for pumped storage unit at low head area,” *Energy Conversion and Management*, vol. 177, pp. 592–604, 2018.

[7] M. Treuer, T. Weissbach, and V. Hagenmeyer, “Flatness-based feedforward in a two-degree-of-freedom control of a pumped storage power plant,” *IEEE Transactions on Control Systems Technology*, vol. 19, no. 6, pp. 1540–1548, 2011.

[8] C. Li, Y. Mao, J. Yang, Z. Wang, and Y. Xu, “A nonlinear generalized predictive control for pumped storage unit,” *Renewable Energy*, vol. 114, pp. 945 – 959, 2017.

[9] T. Chen, C. Xu, Q. Lin, R. Loxton, and K. L. Teo, “Water hammer mitigation via PDE-constrained optimization,” *Control Engineering Practice*, vol. 45, pp. 54 – 63, 2015.

[10] T. Chen, Z. Ren, C. Xu, and R. Loxton, “Optimal boundary control for water hammer suppression in fluid transmission pipelines,” *Computers & Mathematics with Applications*, vol. 69, no. 4, pp. 275 – 290, 2015.

[11] J. Betts, *Practical Methods for Optimal Control and Estimation Using Nonlinear Programming*, 2nd ed. Philadelphia, USA: SIAM, 2010.

[12] M. Gerdts, *Optimal Control of ODEs and DAEs*. Berlin/Boston: De Gruyter, 2012.

[13] C. Canuto, M. Y. Hussaini, A. Quarteroni, and T. A. Zang, *Spectral Methods: Fundamentals in Single Domains*, ser. Scientific Computation. Berlin, Germany: Springer, 2006.

[14] C. Canuto, M. Y. Hussaini, A. Quarteroni, and T. Zang, *Spectral methods: Evolution to Complex Geometries and Applications to Fluid Dynamics*, ser. Scientific Computation. Berlin, Germany: Springer, 2007.

[15] J.-F. Mennemann, J. Schmidt, W. Kemmetmüller, and A. Kugi, “Simulation of wave effects in pumped-storage power plants using the spectral element method (in german),” *at-Automatisierungstechnik*, vol. 64, no. 8, pp. 681–695, 2016.

Post-print version of the article: J. Mennemann, L. Marko, J. Schmidt, W. Kemmetmüller, and A. Kugi, “Nonlinear model predictive control of a variable-speed pumped-storage power plant,” *IEEE Transactions on Control Systems Technology*, vol. 29, no. 2, pp. 645–660, 2021. DOI: 10.1109/TCST.2019.2956910
The content of this post-print version is identical to the published paper but without the publisher’s final layout or copy editing.

[16] J.-F. Mennemann, L. Marko, J. Schmidt, W. Kemmetmüller, and A. Kugi, "The spectral element method as an efficient tool for transient simulations of hydraulic systems," *Applied Mathematical Modelling*, vol. 54, pp. 627–647, 2018.

[17] E. B. Wylie and V. L. Streeter, *Fluid Transients in Systems*. Englewood Cliffs: Prentice-Hall, 1993.

[18] T. Wu and C. C. Ferng, "Effect of nonuniform conduit section on waterhammer," *Acta Mechanica*, vol. 137, no. 3-4, pp. 137–149, 1999.

[19] M. S. Ghidaoui, M. Zhao, D. A. McInnis, and D. H. Axworthy, "A Review of Water Hammer Theory and Practice," *Appl. Mech. Rev.*, vol. 58, pp. 49–76, 2005.

[20] M. H. Chaudhry, *Applied Hydraulic Transients*, 3rd ed. New York, USA: Springer, 2014.

[21] W. Zielke, "Frequency-dependent friction in transient pipe flow," *Journal of Basic Engineering*, vol. 90, no. 1, pp. 109–115, 1968.

[22] A. Adamkowski, "Analysis of transient flow in pipes with expanding or contracting sections," *Journal of Fluids Engineering*, vol. 125, no. 4, pp. 716–722, 2003.

[23] A. Adamkowski and M. Lewandowski, "Experimental examination of unsteady friction models for transient pipe flow simulation," *Journal of Fluid Engineering*, vol. 128, pp. 1351–1363, 2006.

[24] C. Nicolet, "Hydroacoustic modelling and numerical simulation of unsteady operation of hydroelectric systems," Ph.D. dissertation, EPFL, Lausanne, Switzerland, 2007.

[25] C. Nicolet, F. Avellan, P. Allenbach, A. Sapin, and J.-J. Simond, "New tool for the simulation of transient phenomena in Francis turbine power plants," in *Proc. of the Hydraulic Machinery and Systems 21st IAHR Symposium*, Lausanne, Switzerland, Sep. 2002.

[26] A. Goshtasby and W. Oneill, "Curve fitting by a sum of gaussians," *CVGIP: Graphical Models and Image Processing*, vol. 56, no. 4, pp. 281 – 288, 1994.

[27] P. C. Krause, O. Wasynczuk, and S. D. Sudhoff, *Analysis of Electric Machinery and Drive Systems*. New York, USA: Wiley, 2002.

[28] Q. Gong, W. Kang, and I. M. Ross, "A pseudospectral method for the optimal control of constrained feedback linearizable systems," *IEEE Transactions on Automatic Control*, vol. 51, no. 7, pp. 1115–1129, July 2006.

[29] Q. Gong, F. Fahroo, and I. Ross, "Spectral algorithm for pseudospectral methods in optimal control," *Journal of Guidance, Control, and Dynamics*, vol. 31, no. 3, pp. 460–471, May–June 2008.

[30] L. Marko, J.-F. Mennemann, L. Jadachowski, W. Kemmetmüller, and A. Kugi, "Early- and late-lumping observer designs for long hydraulic pipelines: Application to pumped-storage power plants," *International Journal of Robust and Nonlinear Control*, vol. 28, no. 7, pp. 2759–2779, 2018.

[31] R. K. Mandela, R. Rengaswamy, S. Narasimhan, and L. N. Sridhar, "Recursive state estimation techniques for nonlinear differential algebraic systems," *Chemical Engineering Science*, vol. 65, no. 16, pp. 4548 – 4556, 2010.

[32] J. Andersson, J. Åkesson, and M. Diehl, "Dynamic optimization with CasADi," in *2012 IEEE 51st IEEE Conference on Decision and Control (CDC)*, 2012, pp. 681–686.

[33] J. A. E. Andersson, J. Gillis, G. Horn, J. B. Rawlings, and M. Diehl, "CasADi: a software framework for nonlinear optimization and optimal control," *Mathematical Programming Computation*, Jul 2018. [Online]. Available: https://doi.org/10.1007/s12532-018-0139-4

[34] A. Wächter and L. T. Biegler, "On the implementation of an interior-point filter line-search algorithm for large-scale nonlinear programming," *Mathematical Programming*, vol. 106, no. 1, pp. 25–57, 2006.

Jan-Frederik Mennemann received the Dipl.-Math. degree in mathematics from the Johannes Gutenberg Universität Mainz, Germany, in 2008 and his Ph.D. (Dr. techn.) in mathematics from the Technische Universität Wien (TU Wien), Vienna, Austria, in 2013. From 2014 to 2017 he worked as a project assistant at the Automation and Control Institute at TU Wien. His research interests include numerical methods for partial differential equations, optimization and control.

Lukas Marko received the Dipl.-Ing. degree in electrical engineering from TU Wien, Vienna, Austria, in 2016. Since 2016, he works as a project assistant in the Christian Doppler Laboratory for Model-Based Process Control in the Steel Industry at the Automation and Control Institute at TU Wien. His research interests include physics-based modeling, numerical methods in engineering and advanced process control.

Jakob Schmidt received the Dipl.-Ing. degree in electrical engineering from TU Wien, Vienna, Austria, in 2012. From 2012 to 2017 he was a project assistant at the Automation and Control Institute at TU Wien, where he worked in the research fields of modeling, simulation, optimized operation and control of pumped storage power plants.

Wolfgang Kemmetmüller (M'04) received the Dipl.-Ing. degree in mechatronics from the Johannes Kepler University Linz, Austria, in 2002, his Ph.D. (Dr.-Ing.) degree in control engineering from Saarland University, Saarbruecken, Germany, in 2007 and the Habilitation degree in system theory and automatic control from TU Wien, Vienna, Austria, in 2016. From 2002 to 2007 he worked as a research assistant at the Chair of System Theory and Automatic Control at Saarland University. From 2007 to 2016 he has been a senior researcher and Assistant Professor at the Automation and Control Institute at TU Wien, Vienna, Austria and since 2016 he is Associate Professor. His research interests include the physics based modeling and the nonlinear control of mechatronic systems with a special focus on electrohydraulic and electromechanical systems.

Andreas Kugi (M'94-SM'19) received the Dipl.-Ing. degree in electrical engineering from TU Graz, Austria, in 1992, the Ph.D. degree in control engineering and the Habilitation degree in automatic control and control theory from Johannes Kepler University (JKU), Linz, Austria, in 1995 and 2000, respectively. He was an Associate Professor with JKU from 2000 to 2002 and a Full Professor with Saarland University, Germany from 2002 to 2007. Since 2007, he has been the Head of the Automation and Control Institute (ACIN), TU Wien, Austria, and since 2017, he is also the Head of the Center for Vision, Automation & Control at the Austrian Institute of Technology (AIT). His main research interests include the modeling, control and optimization of complex dynamical systems, the mechatronic system design as well as robotics and process automation. He is full member of the Austrian Academy of Sciences and member of the German National Academy of Science and Engineering (acatech).

Post-print version of the article: J. Mennemann, L. Marko, J. Schmidt, W. Kemmetmüller, and A. Kugi, "Nonlinear model predictive control of a variable-speed pumped-storage power plant," *IEEE Transactions on Control Systems Technology*, vol. 29, no. 2, pp. 645–660, 2021. DOI: 10.1109/TCST.2019.2956910
The content of this post-print version is identical to the published paper but without the publisher's final layout or copy editing.